

Sensitivity of MJO simulations to diabatic heating profiles

Chongyin Li · Xiaolong Jia · Jian Ling ·
Wen Zhou · Chidong Zhang

Received: 3 May 2007 / Accepted: 11 August 2008 / Published online: 2 September 2008
© Springer-Verlag 2008

Abstract The difficulty for global atmospheric models to reproduce the Madden–Julian oscillation (MJO) is a long-lasting problem. In an attempt to understand this difficulty, simple numerical experiments are conducted using a global climate model. This model, in its full parameterization package (control run), is capable of producing the gross features of the MJO, namely, its planetary-scale, intraseasonal, eastward slow propagation. When latent heating profiles in the model are artificially modified, the characteristics of the simulated MJO changed drastically. Intraseasonal perturbations are dominated by stationary component over the Indian and western Pacific Oceans when heating profiles are top heavy (maximum in the upper troposphere). In contrast, when diabatic heating is bottom

heavy (maximum in the lower troposphere), planetary-scale, intraseasonal, eastward propagating perturbations are reproduced with a phase speed similar to that of the MJO. The difference appears to come from surface and low-level moisture convergence, which is much stronger and more coherent in space when the heating profile is bottom heavy than when it is top heavy. These sensitivity experiments, along with other theoretical, numerical, and observational results, have led to a hypothesis that the difficulty for global models to produce the MJO partially is rooted in a lack of sufficient diabatic heating in the lower troposphere, presumably from shallow convection.

1 Introduction

The tropical intraseasonal oscillation is an important element of the atmospheric climate system. One of its dominant components is the eastward moving Madden–Julian oscillation (MJO, Madden and Julian 1971, 1972). A related component is the northward moving intraseasonal variation associated with the Asian summer monsoon (e.g., Krishnamurti and Subrahmanyam 1982; Li 1985; Wang and Rui 1990; Li et al. 2001). The importance of the MJO to tropical and global weather and climate has been increasingly appreciated. The MJO influences onset and breaks of the summer monsoons over Asia (Lau and Chan 1986; Mu and Li 2000; Lawrence and Webster 2002), Australia (Hendon and Liebmann 1990; Wheeler and McBride 2005), Americas (Paegle et al. 2000; Higgins and Shi 2001), and Africa (Matthews 2004). It has been suggested that the evolution of the ENSO can be affected by the MJO (e.g., Lau and Shen 1988; Li and Zhou 1994; Kessler et al. 1995; Li and Long

C. Li · X. Jia · J. Ling
Laboratory for Numerical Modeling for Atmospheric Sciences
and Geophysical Fluid Dynamics, Institute of Atmospheric
Physics, Chinese Academy of Sciences, Beijing, China

C. Li
Institute of Meteorology, PLA University of Science
and Technology, Nanjing, China

X. Jia
National Climate Center, China Meteorological Administration,
Beijing, China

J. Ling · W. Zhou
City U-IAP Laboratory for Atmospheric Sciences, Department
of Physics and Materials Science, City University of Hong Kong,
Hong Kong, China

C. Zhang (✉)
University of Miami, 4600 Rickenbacker Causeway,
MPO, Miami, FL 33149, USA
e-mail: czhang@rsmas.miami.edu

2002; Zhang and Gottschalck 2002). Tropical extreme events, such as cyclogenesis, can be modulated by the MJO (Liebmann et al. 1994; Maloney and Hartmann 2000; Mo 2000; Bessafi and Wheeler 2006; Frank and Roundy 2006). Many weather and climate phenomena outside the tropics are also related to the MJO (e.g., Li and Li 1997; Bond and Vecchi 2003).

There is no doubt that accurate simulations and prediction of the MJO would lead to tremendous societal benefit. However, current numerical prediction skill of the MJO becomes useless after 15 days (e.g., Waliser et al. 2003), which is far shorter than the dominant timescales of the MJO (30–60 days). Most global climate models (GCMs) fail to reproduce the most salient features of the MJO, such as its intraseasonal timescales and eastward propagation (Slingo et al. 1996; Lin et al. 2006). Our inability of explaining the difficulty of simulating the MJO by current state-of-art GCMs in terms of existing MJO theories reflects our lack of understanding of its fundamental dynamics. The purpose of this study is to explore a particular physical process that might be important to the dynamics and numerical simulations of the MJO: the vertical structure of diabatic heating.

Several mechanisms have been proposed for the MJO (see summaries in Wang 2005 and Zhang 2005). Deep convection has always been taken as the central factor for the MJO. Its roles in the MJO may come in play through interactions with boundary-layer moisture convergence (e.g., Li 1985; Lau and Peng 1987; Wang 1988), tropospheric water vapor (e.g., Grabowski and Moncrieff 2005), cloud radiation (Hu and Randall 1994; Raymond 2001), and sea surface temperature (SST) (e.g., Flatau et al. 1997; Waliser et al. 1999). It is commonly thought that deficiencies in parameterizations of deep convection in GCMs are responsible for model incapability of reproducing the MJO (Li and Smith 1995; Slingo et al. 1996). The sensibility of MJO simulations to convective parameterizations has been well demonstrated (Wang and Schlesinger 1999). However, it is uncertain exactly what inadequacy in convective parameterizations contributes most to the deterioration in MJO simulations. This study investigates the dependence of numerical simulations of the MJO on the vertical structure of diabatic heating.

It has been documented that diabatic heating profiles in GCMs are typically deep, with peaks in the mid to upper troposphere (Lin et al. 2004), in contrast to the observed top-heavy profile typical for tropical convective systems dominated by stratiform rain (e.g., Houze 1989). This poses an intriguing question: Is the lack of top-heavy heating profiles in GCMs responsible for their inability of reproducing a realistic MJO? The modeling

experiments in this study indicate the opposite: it is bottom-heavy heating profile with its maximum in the lower to mid troposphere that might play a crucial role in simulating a realistic MJO, especially its eastward propagation.

The importance of diabatic heating in the lower troposphere to the MJO was first suggested by Li (1983). He showed that characteristics of tropical unstable modes were sensitively related to the vertical structure of diabatic heating (see more discussion in Sect. 5). The linear theory of the equatorial waves (Matsuno 1966) predicts that the phase speed of the eastward-propagating Kelvin wave is $c = (gh)^{1/2}$, where g is gravity and h the equivalent depth, a measure of the vertical scale. In this theory, h is determined by the vertical scale of diabatic heating, the source of energy for the tropospheric Kelvin wave. A smaller h due to a shallow heating profile leads to a slower phase speed. It has been shown that slow wave-CISK modes can indeed be produced by heating profiles peaking in the lower troposphere, namely, between 500 and 700 hPa (Lau and Peng 1987; Chang and Lim 1988; and Sui and Lau 1989).

Low-level heating may come from shallow precipitating clouds that are abundant in the western equatorial Pacific prior to the deep convective phase of the MJO (e.g., Johnson et al. 1999). It has been hypothesized that these shallow convective clouds may be instrumental to moistening the lower troposphere and set a stage favorable to the following deep convective phase of the MJO (e.g., Slingo et al. 2003). This current study provides new modeling evidence that lower-tropospheric heating is in favor of the MJO and points out a possible role of shallow convective clouds in the MJO through their diabatic heating structure in addition to their moistening effects.

A comparison of three simulations by two GCMs with different cumulus parameterization schemes (Sect. 2) indicates that the one with stronger diabatic heating in the lower troposphere produced a more realistic MJO (Sect. 3). In simple numerical experiments, vertical heating profiles in a GCM were artificially modified to be top heavy (maximum in the upper troposphere) or bottom heavy (maximum in the lower troposphere). Slow eastward propagating intraseasonal perturbations with a deep, first baroclinic mode structure, interpreted as of the MJO, were produced only when diabatic heating is bottom heavy. When diabatic heating is top heavy, the dominant intraseasonal perturbations became stationary (Sect. 4). These results, together with their diagnoses and other numerical, theoretical and observations results (Sect. 5), lay the foundation for a hypothesis that a lack of diabatic heating in the lower troposphere is a reason for many GCMs to fail in reproducing a realistic MJO (Sect. 6).

2 Model and methodology

2.1 Models

Two global atmospheric models were used in this study. One is the atmospheric component of the Flexible Global Ocean–Atmosphere–Land System model (FGOALS), which was originally from the version of Simmonds (1985) and developed at the Institute of Atmospheric Physics (IAP) Laboratory for Numerical Modeling for Atmospheric Sciences and Geophysical Fluid Dynamics (LASG) (Wu et al. 1996). This is a global spectral model of R42 (128×108 Gaussian grid points, equivalent resolution of 2.8125° longitude \times 1.66° latitude) and nine sigma levels with the top level at 17 hPa (R42L9). It employs a unique dynamic core that removes a reference atmosphere to reduce systematic errors due to truncation and topography (Wu 1997). The parameterization package includes the Slingo et al. (1996) scheme for radiation, the Slingo (1980, 1987) scheme for cloud diagnosis, the Holtslag and Boville (1993) scheme for the boundary layer, and the moisture convective adjustment scheme of Manabe et al. (1965). A simplified version of the Simple Biosphere model (SIB) of Sellers et al. (1986) is used for the land surface processes (Xue et al. 1991). A semi-implicit scheme with a time step of 15 min was used. This model will be referred to as SAMIL. Further details on the formulation of SAMIL are available in Wu et al. (1996), Wu (1997) and Wang et al. (2005).

The other model used is the NCAR Community Atmosphere Model (CAM2.0.2) with the Euler dynamic core of T42 (128×64 Gaussian grid points), 26 vertical levels (top level at 2.917 hPa). The integration scheme is semi-implicit with a time step of 20 min. Standard parameterization package (Collins et al. 2006) was used, except in one simulation where the Zhang and McFarlane (1995) scheme (ZM scheme) in the CAM original package was replaced by the Tiedtke (1989) scheme (T scheme). The original version of CAM with the ZM scheme will be referred to as CAM2+ZM. The modified version using the T scheme will be referred to as CAM2+T.

2.2 Experiment and analysis

Both models were integrated for January 1, 1978–December 31, 1989. Initial conditions were based on the NCAR/NCEP reanalysis (Kalney et al. 1996) for SAMIL and a previous simulation up to January 1, 1987 for CAM2. Time-evolving monthly mean sea surface temperature (SST) and sea ice from Program for Climate Model Diagnostic and Intercomparison (PCMDI) were used in both models. The first year of integration was ignored for diagnostics, thus the model data sets cover 11 years for

January 1979–December 1989. The NCAR/NCEP reanalysis and Xie and Arkin (1997) precipitation data (hereafter referred to as XA precipitation) were used to validate the model simulations.

Main diagnostic variables include zonal wind at the 850 hPa level (U850) and 200 hPa level (U200), velocity potential at the 200 hPa level (X200), and precipitation. Anomalous time series were first created by removing the respective 11-year climatology from daily mean data. Then a 30–60 day band-pass filter was applied to isolate the intraseasonal variability. Power spectra, empirical orthogonal function (EOF), and linear regression were used to analyze simulated MJO features.

3 Simulations of the MJO

Detailed descriptions of the mean and MJO simulated by SAMIL and the two CAM models are given by Jia (2006). Here, only the main features of the simulated MJO are discussed. The most prominent feature of the MJO, namely, its slow eastward propagation, is captured by SAMIL. Figure 1 compares lag regression of band-pass (30–60 day) filtered U200, X200, and U850 based on the NCEP reanalysis (left column) and SAMIL (right). The eastward propagation of the MJO reproduced by SAMIL is evident, although the phase speed is slightly higher than in the reanalysis, especially in the western hemisphere. The ability of SAMIL to reproduce the MJO is further demonstrated by an EOF analysis. The first two leading EOF modes of band-pass (30–60 day) filtered U850 is in quadrature with each other, as expected for the MJO in the reanalysis (Fig. 2). Their lag correlation reaches the maximum at 9 days, suggesting a period of 36 days. This is shorter than the 44 day period indicated by the maximum lag correlation at 11 days between the first two leading EOF modes in the reanalysis U850. This has been a common problem in MJO simulations for many years (e.g., Slingo et al. 1996). Only few GCMs are able to reproduce the realistic MJO phase speed (e.g., Maloney and Hartmann 1998; Sperber et al. 2005; Zhang et al. 2006).

The agreement and discrepancy between the MJO in SAMIL and the reanalysis can be further seen from their time-space spectra (Fig. 3). An intraseasonal spectral peak near 50–60 days and well separated from the lower frequency power exists clearly for both NCEP U850 and XA precipitation. In the simulation of SAMIL, such spectral peaks can be discerned, if weaker than in the reanalysis and observations. Meanwhile, there are additional spectral peaks near 30 days in SAMIL U850 and precipitation with roughly equal strength as the intraseasonal peaks. This exaggeration of the spectral power near 30 days is another common problem in GCMs (e.g., Zhang et al. 2006). They

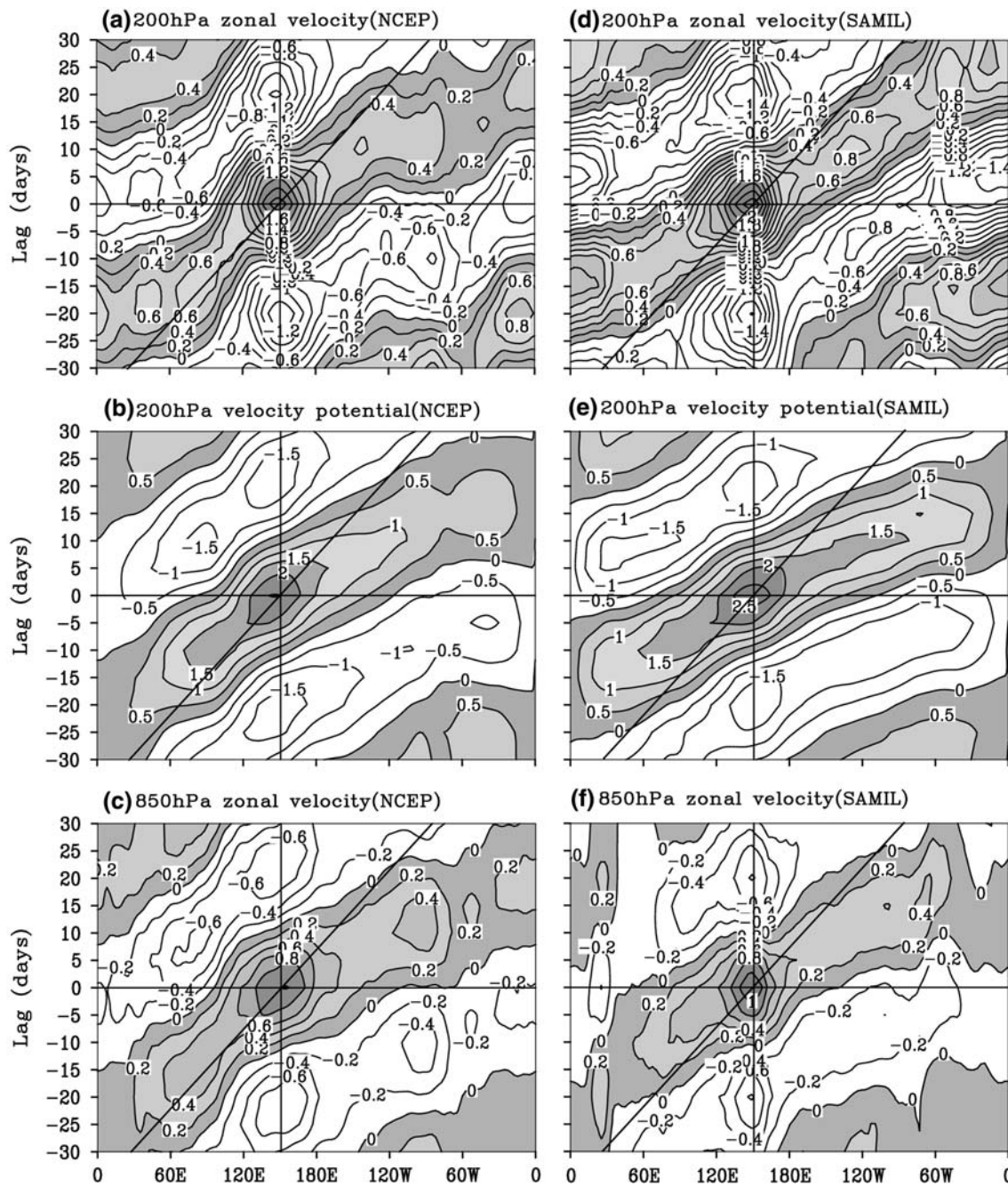


Fig. 1 Lag regression of band-pass (30–60 day) filtered U200 (m s^{-1} , upper panels), 200 hPa velocity potential ($10^6 \text{ m}^2 \text{ s}^{-2}$, middle), and U850 (m s^{-1} , lower) with the reference point at

150°E , all averaged over 10°S – 10°N based on the NCEP reanalysis (left column) and SAMIL (right). Positive values are shaded. The straight lines indicate 5 m s^{-1} phase speed

are partially responsible for the shorter period and faster eastward phase speed of the simulated MJO. Another problem in the simulation is the lack of eastward moving spectral power at zonal wavenumber two ($k = 2$) in precipitation. In observations, such spectral power exist with the same amplitude as at $k = 1$. These problems in the simulation notwithstanding, the most important feature for the MJO in the spectra of NCEP U850 and XA

precipitation is well reproduced by SAMIL: the eastward moving power at the planetary scale ($k = 1$) and intra-seasonal period (30–60 days) is much greater than its westward moving counterpart. Most current GCMs fail to reproduce this salient property of the MJO (e.g., Lin et al. 2006). There is hardly any GCM that can produce much more realistic MJO spectrum than SAMIL (Zhang et al. 2006).

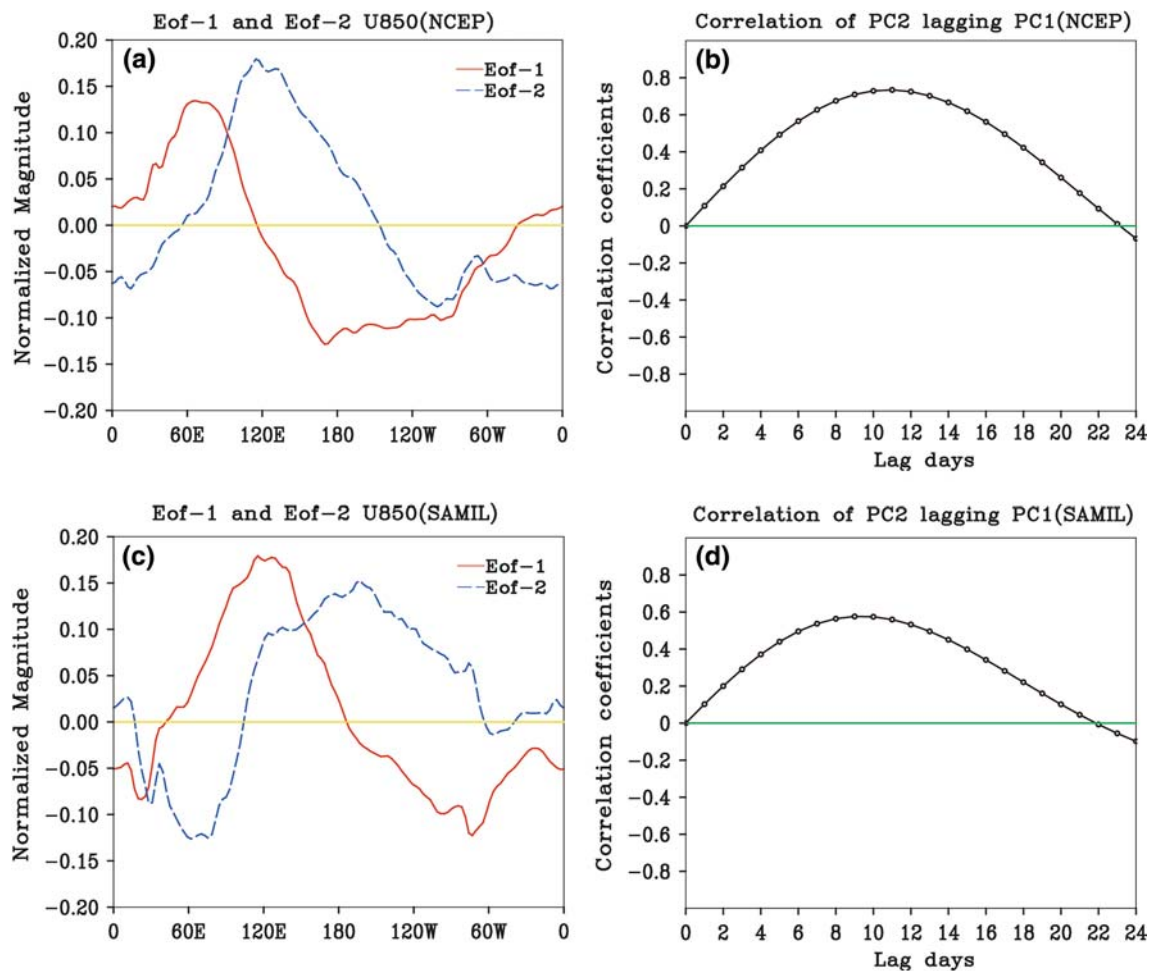


Fig. 2 PCs of the first two leading EOF for band-pass (30–60 day) filtered U850 (*left column*) and their lag correlation (*right column*) based on the NCEP reanalysis (*top row*) and SAMIL (*bottom*)

The ability of CAM+ZM and CAM+T to reproduce observed features of the MJO is much limited than that of SAMIL. While there is a faint hint of eastward propagation in band-pass filtered U200, such hint disappears for X200 and U850 (Fig. 4). There are even strong signs of westward propagation in U850 of CAM+ZM. The time-space spectra of CAM+ZM indeed show stronger westward moving power than eastward moving one for U850 (Fig. 5). Replacing the ZM cumulus scheme by the T scheme apparently increased the eastward moving power. But the resulting spectra remain highly unrealistic. One example is the lack of eastward moving power at $k = 1$ for precipitation. It is interesting to notice that other GCMs with the T scheme are able to produce much more realistic MJOs than CAM+T (Zhang et al. 2006). This suggests that, while cumulus scheme is a critical component of a model for its ability of reproducing the MJO, it alone is not always the determining factor.

These simulations exemplify the intriguing puzzle: What is the most critical factor determining the success and

failure of a model to reproduce the MJO and why MJO simulations are so sensitive to cumulus parameterizations? In the next section, we will present simple numerical experiments to demonstrate that the vertical structure of diabatic heating might be one piece of the puzzle.

4 Sensitivity to heating profiles

There might be various reasons for the SAMIL and CAM2 simulations to be different. Here, we consider their different vertical structures of diabatic heating. The mean diabatic heating profiles over the western Pacific (140–160°E, 10°N–10°S) during periods with strong precipitation from the three simulations introduced previously are compared in Fig. 6. They indeed exhibit different characteristics. The heating profile had a peak near the 600 hPa level in SAMIL, near the 400–450 hPa levels in CAM2+ZM, and near the 550 hPa level in CAM2+T. The maximum heating is the strongest in CAM2+T (10 K/day) and much weaker in

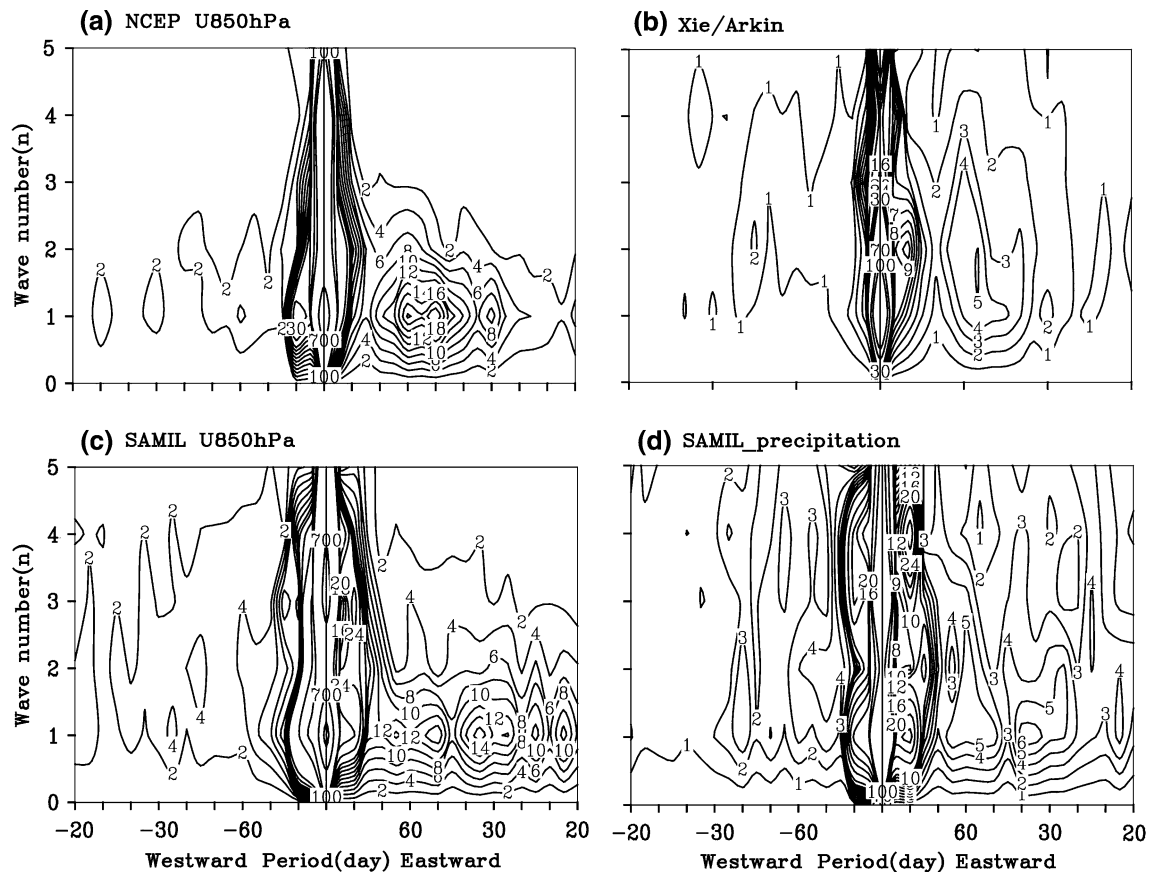


Fig. 3 Time–space spectra of **a** NCEP U850 ($\text{m}^2 \text{s}^{-2}$), **b** XA precipitation ($\text{mm}^2 \text{day}^{-2}$), **c** U850 from SAMIL ($\text{m}^2 \text{s}^{-2}$), and **d** precipitation from SAMIL ($\text{mm}^2 \text{day}^{-2}$). The U850 contour interval is $2 \text{ m}^2 \text{ s}^{-2}$ for values smaller than and equal to 20 and contours of

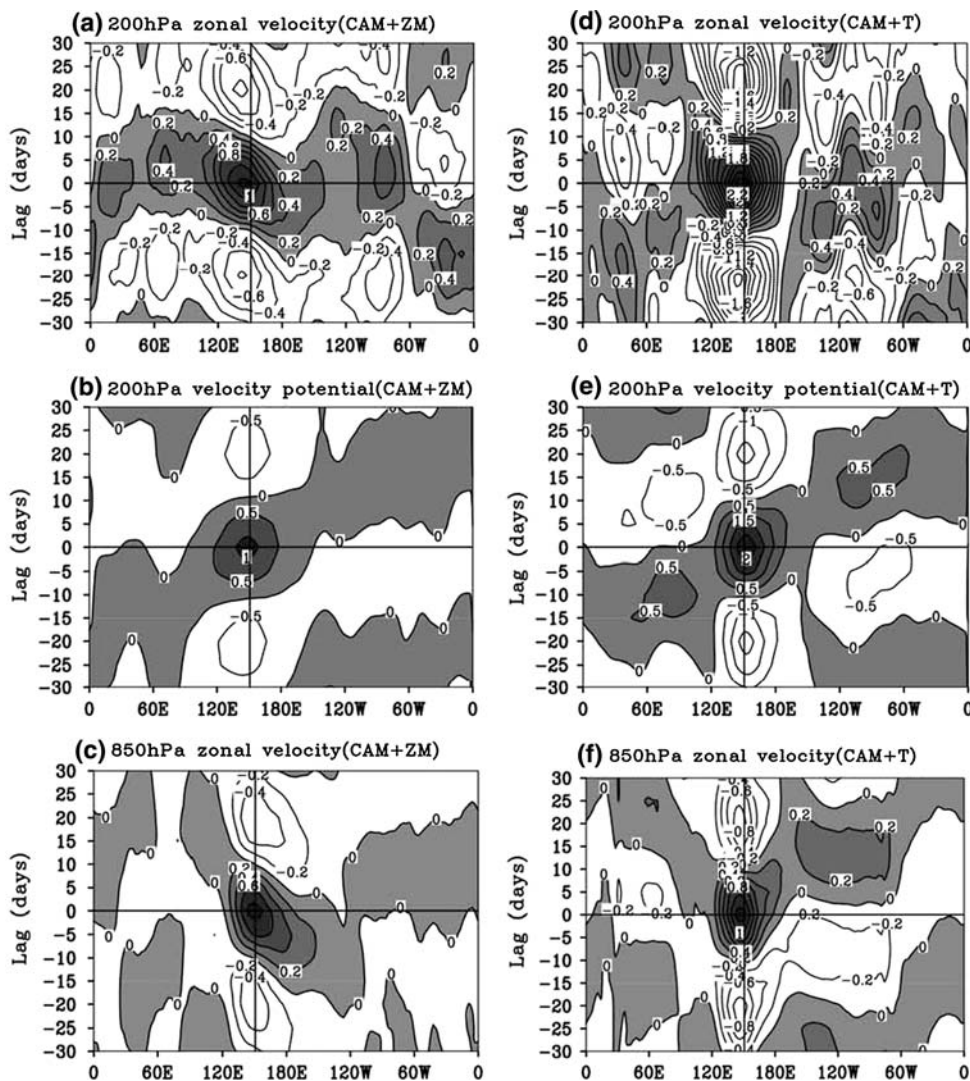
24, 30, 70, 100, 700, 1200 are given for values exceed 20, starting at $2 \text{ m}^2 \text{ s}^{-2}$. The precipitation contour interval is $1 \text{ mm}^2 \text{day}^{-2}$ for values smaller than and equal to 10 and, contours of 12, 16, 20, 24, 30, 70, 100, 700 are given for values exceed 10

SAMIL and CAM2+ZM (5 K/day). While the heating profiles of CAM2 are typical of GCMs, the heating profile of SAMIL is unusual in that there is a minimum near the 450 hPa level. All the three, meanwhile, miss the top-heavy structure (peak at and above the 200 hPa level) found in observation during the convective peak phase of the MJO (Lin et al. 2004). Another interesting difference among the three heating profiles is that there is a smaller fraction of total heating concentrated in the lower troposphere in CAM2+T and CAM2+ZM than in SAMIL which produced much more realistic MJO signals.

The distinctions among the three heating profiles led to a speculation that, among other things, it was the larger fraction of lower-tropospheric diabatic heating in SAMIL that made its simulation of the MJO more realistic than the other two. This speculation was examined by a set of simulations using SAMIL in which latent heating profiles in the tropics were artificially modified to make them top heavy or bottom heavy. This was done in the following way: to make a given latent heating profile (e.g., solid line in Fig. 7a) top heavy, for example, its amplitude is reduced

by 90% at all levels except at levels six and seven, which correspond roughly to 300 and 250 hPa. The modified profile is the dashed line in Fig. 7a. Then the amplitude of the new profile is amplified at the two peak levels (dashed line in Fig. 7b) so that the vertically integrated latent heating is the same as the original one. In this procedure, cooling at any level in the original profile remains intact. This was done to all latent heating profiles within 20°S and 20°N . Between 20 and 30 degree latitudes, the reduction in amplitude of original latent heating profiles was tapered from 90% gradually to zero and beyond 30 degree latitudes no latent heating profile was modified. The same procedure was followed to create bottom-heavy latent heating profiles except the peak levels are four and five (600 and 500 hPa). Once a latent heating profile was modified, it was added to other diabatic heating terms before total diabatic heating was introduced into the thermodynamic equation. As will be seen below, this procedure effectively changes the vertical structure of total diabatic heating. Notice that when latent heating profiles are modified this way, the moistening effect of clouds is not directly changed.

Fig. 4 Lag regression for band-pass (30–60 day) filtered U200 (upper row), X200 (middle), and U850 (bottom), all averaged over 10°S–10°N, from CAM+ZM (left column) and CAM+T (right). The reference point is at 150°E



Two numerical experiments were made in addition to the control run (CT) in which latent heating profiles generated by the model were not modified. In one experiment, latent heating profiles are modified at each time step and each grid to be top heavy as described above. This run will hereafter be referred to as TH (top heavy). The other experiment is the bottom-heavy counterpart of TH, which will be referred to as BH. Each simulation lasts for 11 years and diagnostics were made for the last 10 years.

The mean tropical (15°N–15°S) total diabatic heating profiles from the three simulations are shown in Fig. 8. The artificial modification of the latent heating profile appears to be highly unrealistic. It may have exaggerated the heating peaks and associated vertical heating gradient for individual profiles (Fig. 7) but not in the mean diabatic heating profiles (Fig. 8). The profiles of CT and BH appear to be similar but one is original without any modification and the other is modified to be bottom heavy in its latent heating component. Realistically, a bottom-heavy heating

profile, due to shallow convection, should have a smaller amplitude than a top-heavy profile due to stratiform rain. But this is not necessarily the case in BH, where bottom-heavy profiles can be as strong as top-heavy ones. The mean profile is even stronger in BH than in TH. The modified profiles in TH and BH, however, form a sharp contrast between extreme cases in which the role of vertical heating profiles in simulations of the MJO can be cleanly isolated and clearly demonstrated, even if exaggerated.

The time evolution of intraseasonal diabatic heating profiles from the three simulations along with their associated zonal-vertical circulations are compared in terms of lag regression in Fig. 9. There is an obvious eastward propagation in diabatic heating and cooling in CT and its associated circulation, with a phase speed about 5.5 m s^{-1} . The associated circulation is of a typical deep, first baroclinic mode extending up to 150 hPa, with mid-level upward motions, low-level convergence and upper-level

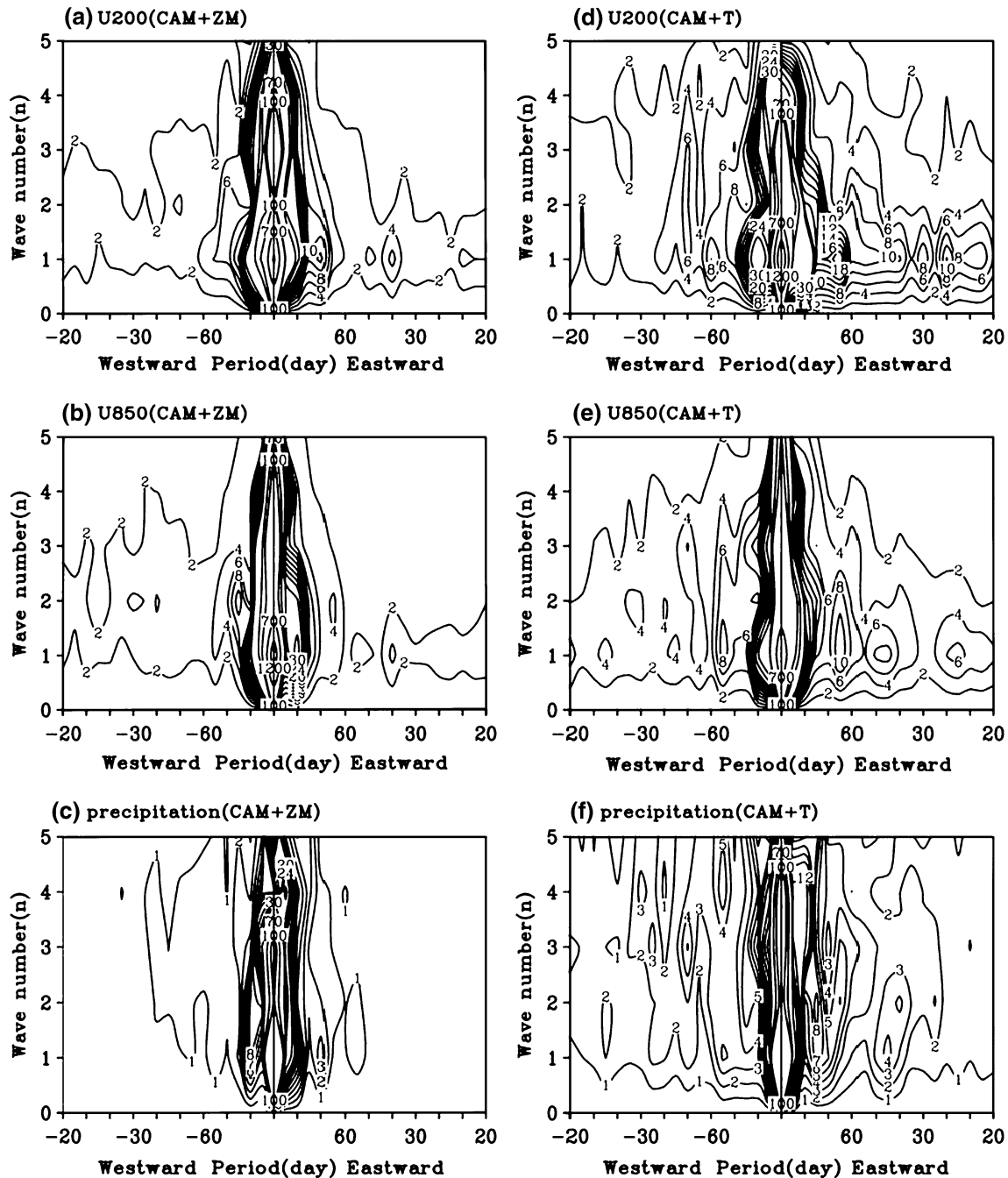


Fig. 5 Time-space spectra of U200 (*upper row*), U850 (*middle*), and precipitation (*bottom*), all averaged over 10°S – 10°N , from CAM+ZM (*left column*) and CAM+T (*right*). Contour intervals same as in Fig. 3

divergence in region of heating, and mid-level downward motions, low-level divergence and upper-level convergence in regions of cooling. The zonal scale of this deep over-turning circulation is about 13,000 km. The time scale of this apparently convection–circulation coupled pattern is clearly 40 days. In the same lag regression but with the reference point at 90°E , there is a visible westward tilt of the upward motion in the heating region (not shown), which as been reported before (e.g., Lin et al. 2006; Kiladis

et al. 2005). There is little doubt that these features represent the MJO.

The manifestation of the MJO in diabatic heating and its associated circulation is completely lost in TH (Fig. 9, middle column). The heating and cooling are weaker and their zonal scales are smaller than in CT. The vertical motion in the mid-troposphere are prominent only in isolated regions. Strong zonal wind is confined to the lower troposphere. The overturning circulation is not only weaker

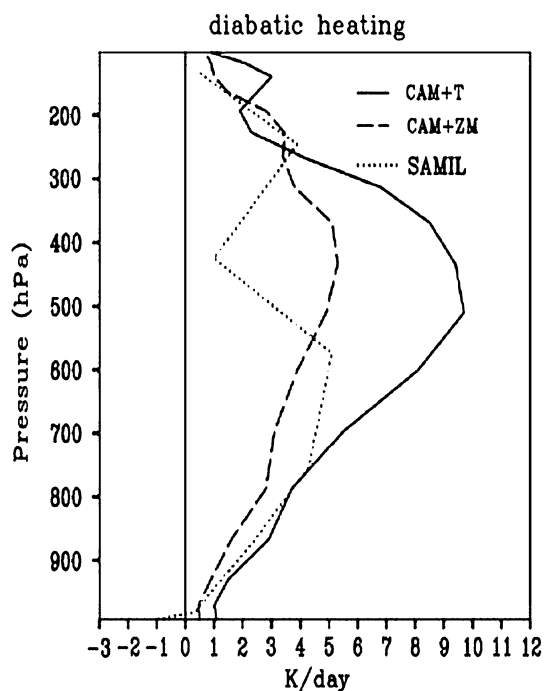


Fig. 6 Mean diabatic heating profile in the western Pacific (140–160°E, 10°S–10°N) during the peak of TIO precipitation from SAMIL (dotted line), CAM2+ZM scheme (dashed), and CAM2+T (solid)

but also shallower than in CT and the large-scale, deep, first mode baroclinic circulation seen in CT is missing here. In a sense, the low-level and upper-level winds are almost decoupled. Furthermore, there is no obvious eastward propagation in either diabatic heating or the circulation. Evidently, no MJO is produced in TH.

Results from BH (Fig. 9, right column) are very similar to those from CT. Especially, the characteristics of the MJO in diabatic heating and wind, namely, the eastward slow propagating large-scale, deep over-turning circulation

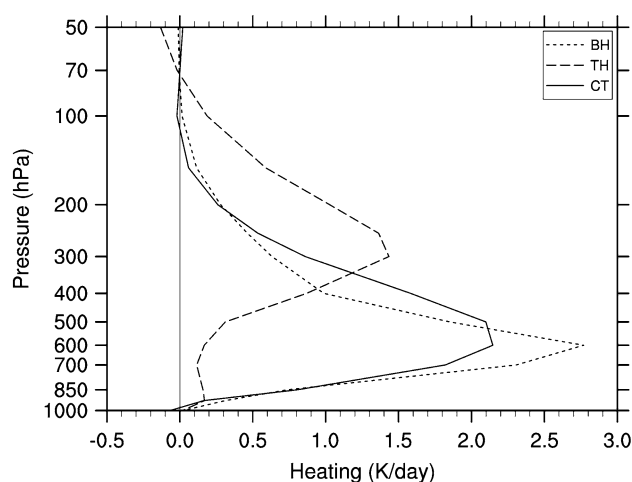
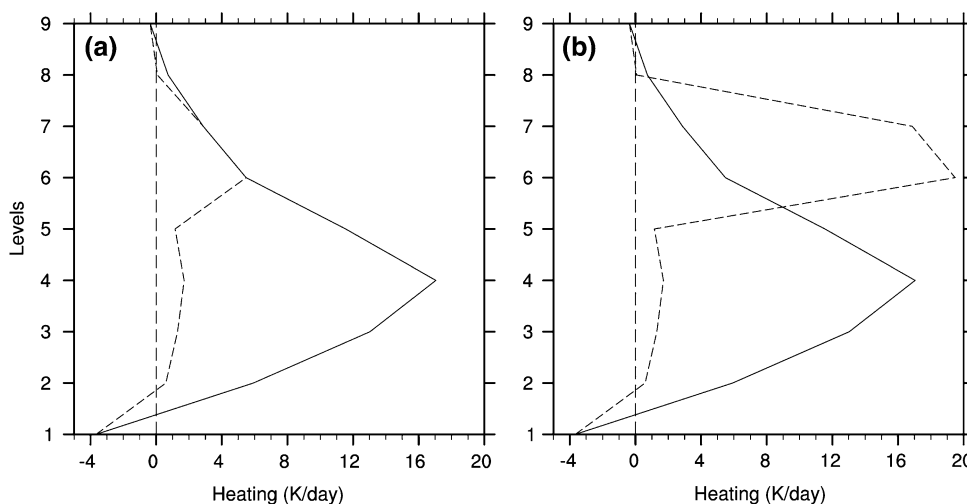


Fig. 8 Mean diabatic heating profiles (K/day) for CT (solid), TH (dashed) and BH (dotted) averaged over 15°N and 15°S

coupled to diabatic heating, are well reproduced in BH. It is interesting to notice that in BH, even though latent heating profiles in the tropics were modified to be bottom heavy, diabatic heating manages to penetrate into the upper troposphere occasionally, in particular, near the reference point (150°E). This presumably is due to the tendency of the model cumulus parameterization to produce extraordinarily strong upper-tropospheric latent heating, as seen in CT, that survived somewhat the artificial reduction. The heating maximum is however in the lower troposphere and is much stronger than the maximum in TH. In consequence, strong upward motions are forged and the deep overturning circulation generated. This is in sharp contrast to TH, where latent heating profiles were modified to be top heavy, lower-tropospheric diabatic heating is always very weak. It is therefore justifiable to say that the discrepancies in the circulation and zonal propagation between TH and BH seen in Fig. 9 are mainly due to the

Fig. 7 Example for the procedure of modifying a diabatic heating profile (K/day). **a** An original profile (solid) and a new profile (dashed) whose amplitude is reduced by 90% except at the peak levels (6 and 7 in this case). **b** The final new profile (dashed) whose vertically integrated heating is the same as the original one (solid)



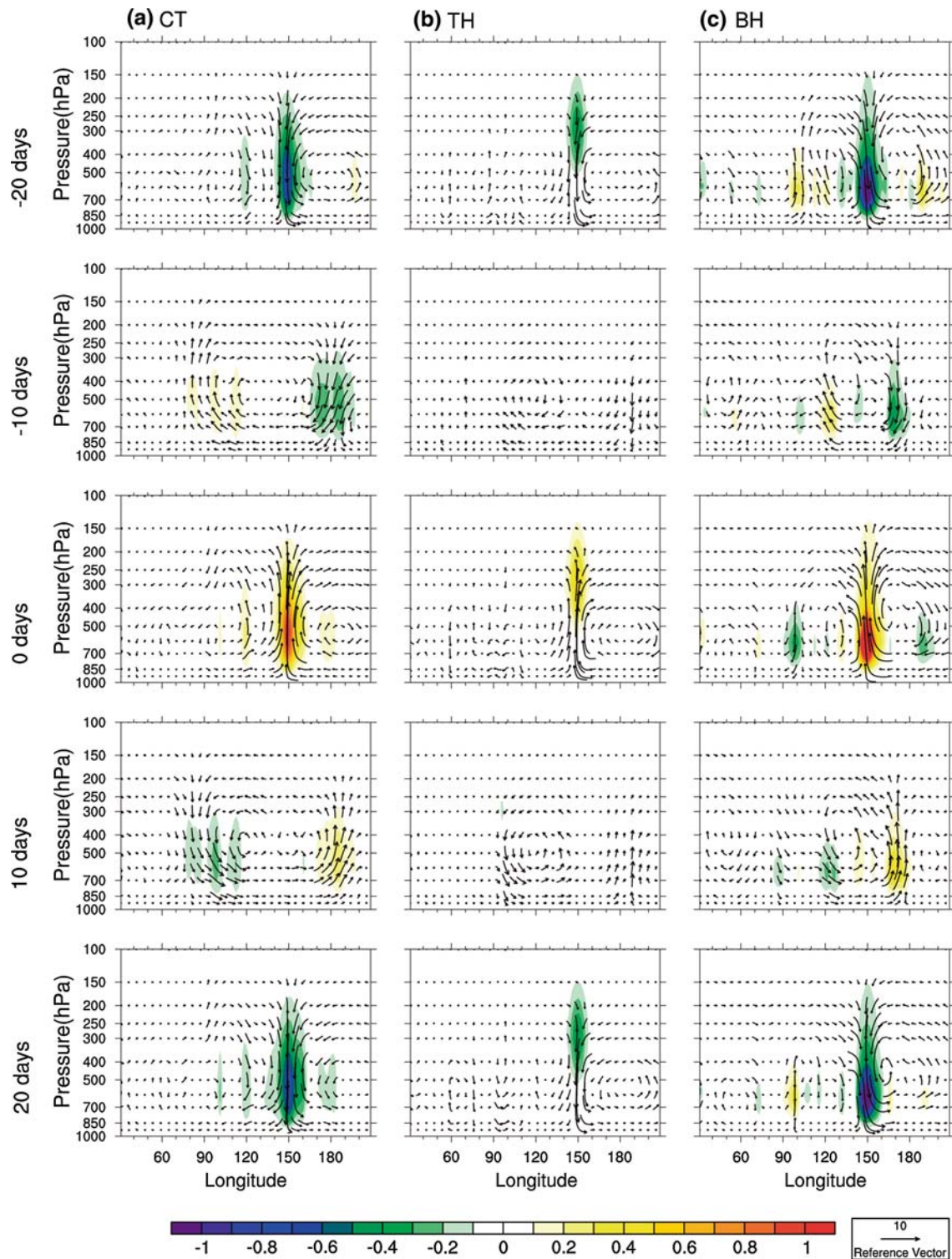


Fig. 9 Lag regression of intraseasonal (30–60 days) diabatic heating (colors, K/day) and zonal-vertical wind vectors in the tropics (15°S–15°N) upon maximum heating at 150°E (0 day) from CT (left column), TH (middle) and BH (right)

difference in lower-tropospheric heating, not in upper-tropospheric heating.

In a more conventional manner, the eastward propagations of intraseasonal U850 along in the three simulations

are demonstrated in Fig. 10 in terms of lag regression. In CT, U850 propagates eastward with a phase speed slightly greater than 5 m s^{-1} over the Indian Ocean but accelerates east of the dateline (Fig. 10a). The fast propagating

($\sim 15 \text{ m s}^{-1}$) perturbations are likely to be free Kelvin waves, which have been seen in the reanalysis wind (Fig. 1c). In TH (Fig. 10b), the slow eastward propagation in U850 over the Indian Ocean seen in CT is almost gone. The intraseasonal perturbations over the western Pacific are more stationary than eastward propagating. The fast eastward propagating Kelvin wave signals east of the dateline remain prominent. In BH (Fig. 10c), the slow eastward propagation over the Indian Ocean is regained with a more realistic phase speed (5 m s^{-1}). Again, the fast propagating Kelvin wave signals east of the dateline are evident. Among the three simulations, BH is the most realistic in comparison to the global reanalysis (Fig. 1c).

The contrast between the intraseasonal eastward propagating perturbations in TH and BH is further demonstrated in Fig. 11, where ratios of eastward versus westward power on intraseasonal (30–60 days) and planetary (zonal wavenumber 1–5) scales are shown for tropical zonal wind and diabatic heating at each level. The large ratios (indicating dominant eastward power and therefore eastward propagation) in zonal wind in the upper (300–200 hPa) and lower (850 hPa) troposphere from CT and BH (Fig. 11a) are obviously associated with the first mode baroclinic structure of the MJO seen in Fig. 9. In TH, eastward power in zonal wind does not dominate westward power at any level. The strong eastward propagating signals in CT and BH is also evident in their diabatic heating fields, but is much stronger in BH than in CT (Fig. 11b). It is interesting that in BH the strongest eastward propagating signal in diabatic heating is confined in the lower troposphere because of the modification whereas the strongest eastward propagating signal in zonal wind is in the upper troposphere. Large-scale dynamics, especially the interaction between the circulation and diabatic heating must play critical roles in establishing the deep vertical structure of zonal wind when diabatic heating is strongest in the lower troposphere. It is striking but consistent to Fig. 9b that there is no dominance of eastward power in diabatic heating in TH at all.

Figure 12 shows time-space spectra of for equatorially symmetric and antisymmetric U850 in a broad range, following Wheeler and Kiladis (1999), to examine the signals of the MJO in the context of other equatorial perturbations. For symmetric perturbations, stronger westward power and weaker eastward power on the MJO scales is evident in TH (Fig. 12c) in comparison to CT (Fig. 12a) and BH (Fig. 12e). They contribute to the lack of dominant eastward power (Fig. 11) and therefore the lack of eastward propagation (Figs. 9b, 10b) in TH. The power for the Kelvin waves is weaker too in TH than in CT and BH. For the Rossby waves, in contrast, the power appears to be slightly stronger in TH than in the other two simulations. Differences in antisymmetric power among the three

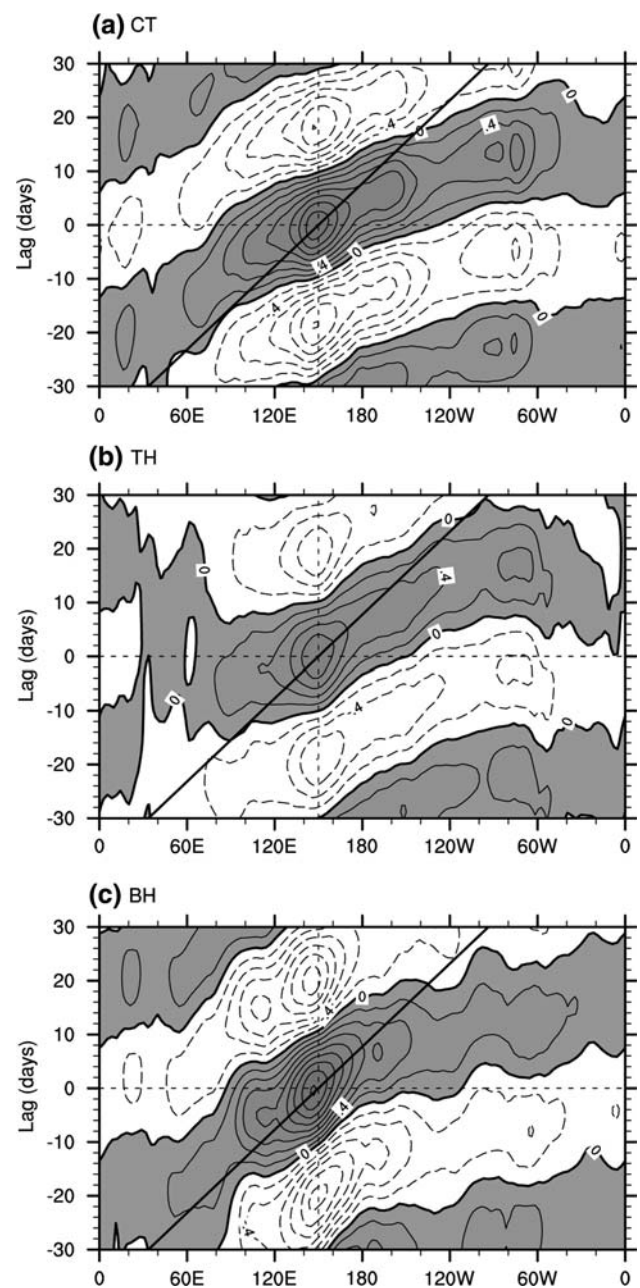


Fig. 10 Lag correlation of band-pass (30–60 day) filtered U850 in the tropics (15°S – 15°N) with reference point at 150°E from **a** CT, **b** TH, and **c** BH. Shading indicates significance at the 99% confidence level. The straight lines indicate 5 m s^{-1} phase speed. Contour interval is 0.2

simulations are marginal. It can be said that the modifications of latent heating profiles in TH and BH did not qualitatively change other equatorial perturbations as they did for the MJO.

In summary, these three experiments clearly demonstrate that intraseasonal eastward propagating perturbations, i.e., the MJO, cannot be produced by the model if its latent heating is always top heavy, but can if its latent heating is

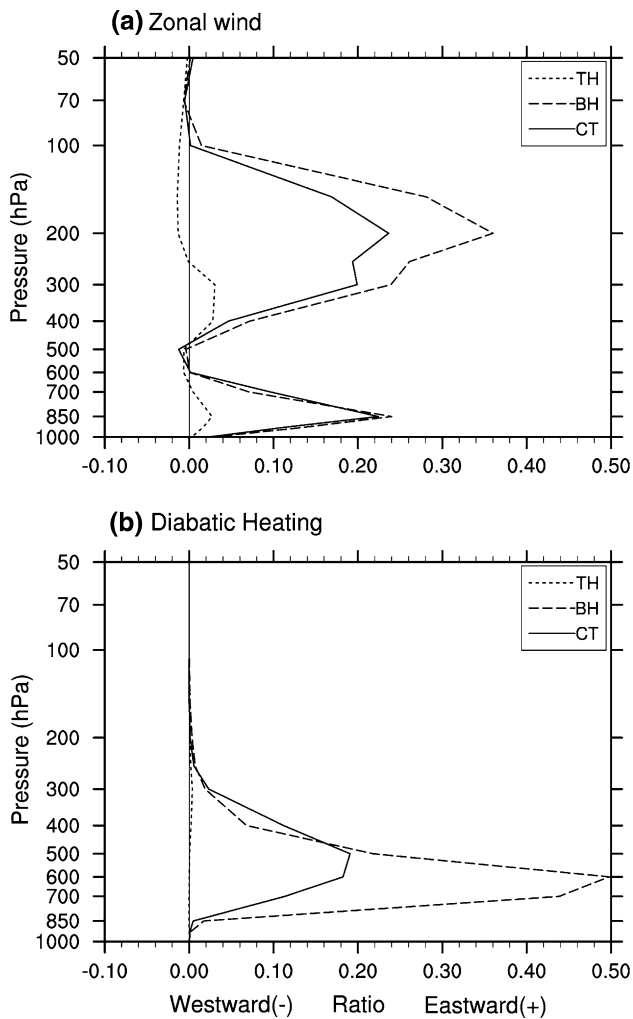


Fig. 11 Ratio of eastward vs. westward power on intraseasonal (30–60 days) and planetary ($k = 1-5$) scales from CT (solid), TH (dashed), and BH (dotted) for **a** zonal wind and **b** diabatic heating, both averaged over $15^{\circ}\text{S}-15^{\circ}\text{N}$

always bottom heavy or is allowed to vary but peaks more often in the lower troposphere than otherwise. This suggests that if a model fails to produce sufficient lower-tropospheric heating, it may not be able to produce a realistic MJO. Possible reasons for the critical role of bottom-heavy heating profile in the MJO are discussed next.

5 Discussion

There could be different reasons for the simulated MJO to be sensitive to diabatic heating profiles. But first, we can rule out the possibility that the difference in the intraseasonal eastward propagation in TH and BH is due to changes in the mean state. The importance of the mean state in a model to its MJO has been suggested (Slingo et al. 1996; Hendon 2000; Slingo et al. (2003); Sperber et al.

2005; Zhang et al. 2006), even though our understanding of this issue remains qualitative and speculative. Mean U850 and precipitation from TH and BH are shown in Fig. 13. Subtle differences in the tropics indeed exist between the two. The most interesting one is an obvious double ITCZ in mean precipitation over the central Pacific in TH (Fig. 13a) but not in BH (Fig. 13b). More investigations on this are certainly warranted because of the large systematic biases in most climate models in this regard. But this is out of the scope of this study. An erroneous double ITCZ may deteriorate the horizontal structure and distribution of a simulated MJO but may not necessarily affect much its eastward propagation (Zhang et al. 2006). Westerly U850 appears to be stronger over the Bay of Bengal in BH than in TH. But both simulations suffer from the biases of too strong easterlies over the equatorial Indian and western Pacific Ocean, a common problem in GCMs (e.g., Zhang et al. 2006). In short, based on our current knowledge of the possible role of the mean state in MJO simulations, there is no obvious reason to expect the difference in the mean state to cause the distinct zonal propagating behaviors of the intraseasonal perturbations in the two simulations as seen in the previous section.

We suggest that the distinct zonal propagating behaviors are caused by the different diabatic heating profiles in the two simulations. To support our suggestion, we first present a simple dynamic argument that may help understand the simulated sensitivity to heating profiles. This argument is based on a study by Li (1983) on tropical wave instability in relation to vertical profiles of convective heating. Results from this study, published in a non-English peer reviewed journal, are unavailable to most readers of this article. The essence of this study is therefore introduced here in the context of the simulated sensitivity described in the previous section.

Without losing generality, tropical wave instability can be studied for a linear atmosphere in an axisymmetric cylinder coordinate system. For the sake of argument, it is assumed that the vertical profile of latent heating rate (Q) can be prescribed, while its amplitude and occurrence are determined by a simple cumulus parameterization, similar to what we have done in our GCM experiments. In this parameterization, Q depends on vertical mass flux due to Ekman pumping and cumulus momentum mixing. When the model atmosphere is divided into a number of pressure layers, an eigenvalue problem can be defined under proper boundary conditions. The solutions to the eigenvalue problem describe the growth rate and vertical structure of corresponding unstable modes.

Four vertical profiles of Q were considered. Three of them have maximum heating rates at certain levels, one is of barotropic structure (Fig. 14). Notice the profiles with

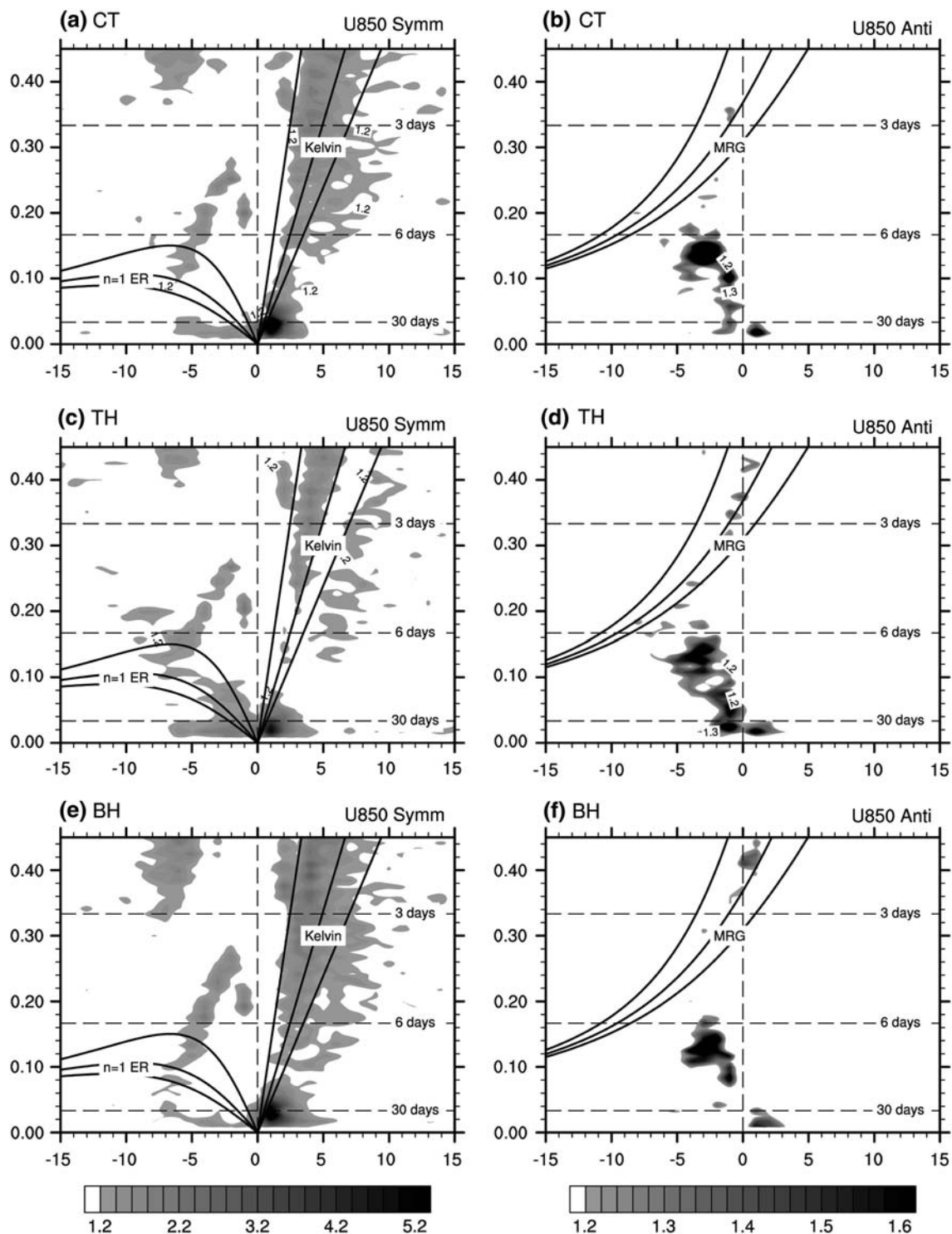


Fig. 12 Space-time spectra for U850 (averaged over 15°S–15°N) from CT (a and b), TH (c and d), and BH (e and f), with the equatorial symmetric components in the left column and asymmetric

components in the right column. Dispersion relation curves of equatorial waves were calculated using equivalent depth $h = 50, 100, 400$ m

maximum heating rates in the upper and lower troposphere are very similar to those in TH and BH of this study (Fig. 8). These vertical profiles of Q lead to distinct characteristics in resulting unstable modes.

The growth rate of unstable modes sensitively depends on the vertical profile of Q , as shown in Fig. 15 where dashed curves represent oscillatory unstable modes, which are relevant to the MJO. A maximum of Q in the mid

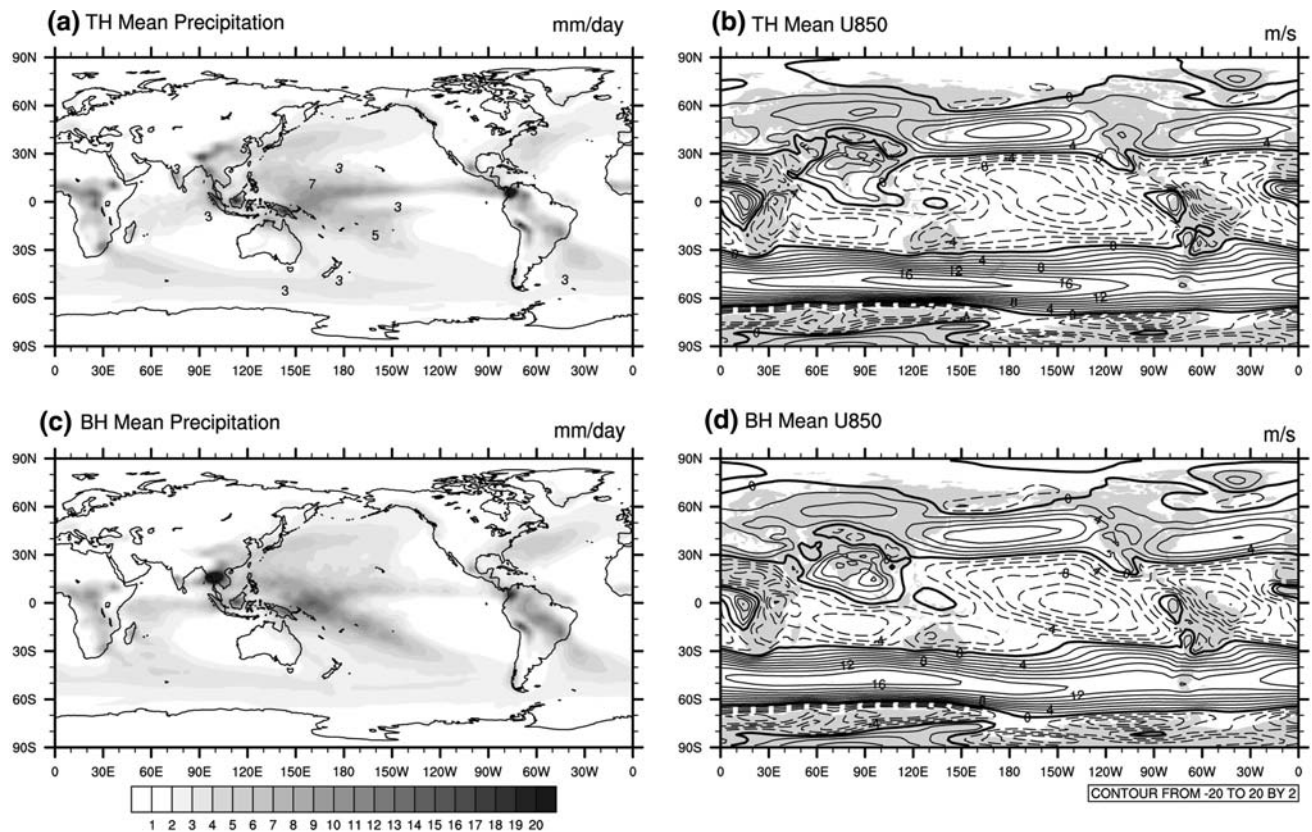


Fig. 13 Mean precipitation from **a** TH and **b** BH and mean U850 from TH (**c**) and BH (**d**)

troposphere gives rise to overall the fastest growth rate at almost all horizontal scales (labeled with 2) but only for non-oscillatory modes. Oscillatory unstable modes occur at very large horizontal scales ($\geq 4,500$ km) regardless of the heating profile. But the growth rate is the largest for heating with its maximum in the lower troposphere (dashed curve labeled with “1” with peak at 4,500 km). At intermediate scales ($< 1,000$ km), oscillatory unstable modes are generated only by low-level heating (curve 1) and barotropic heating (curve 4). Most interestingly, however, the instability catastrophe, namely, the maximum growth rate occurring at the smallest scales (Crum and Dunkerton 1992), is avoided only when the peak of Q is in the lower troposphere (labeled with 1). This wavelength selection of instability is due to convective mixing (friction) in this linear model.

The vertical structures in the vertical and horizontal motions and in temperature also vary with the vertical profiles of Q . The peaks of Q roughly coincide with levels of maximum ascents, reversal levels of horizontal winds, and warm anomalies (not shown). From an energetic point of view, the maxima of both generation of perturbation available potential energy (G) and conversion from perturbation available potential energy to perturbation kinetic energy (K) are roughly in the same layers of maximum Q ,

as anticipated (Fig. 16). While K is the largest for Q with its peak in the upper troposphere (Fig. 16a), G is the largest when maximum Q is in the lower troposphere (Fig. 16c).

These results, as all analytical solutions, critically depend on the assumptions and simplifications applied to the linear atmospheric model. In particular, the cumulus parameterization used in this model may play a dictating role in the solutions. The results from this simple model do not provide any information regarding the propagation direction of the unstable modes. Nevertheless, the solutions to the simple linear atmospheric model suggest that the vertical structure of convective heating rate is important factor to large-scale atmospheric disturbances in response to and interacting with diabatic heating.

Several other studies also explored the role of heating profiles in the intraseasonal oscillation using dynamic framework under wave-CISK assumptions. In a simple dynamical model, Lau and Peng (1987) and Sui and Lau (1989) found that a fast eastward propagating (~ 20 m s $^{-1}$) wave-CISK mode is produced by heating maximized in the upper troposphere (500–200 hPa), while a slow mode with an eastward propagation (7.6 m s $^{-1}$) close to the observed MJO phase speed is produced by heating maximized in the lower troposphere (700–500 hPa). Chang and Lim (1988) obtained quite different results. They found that while

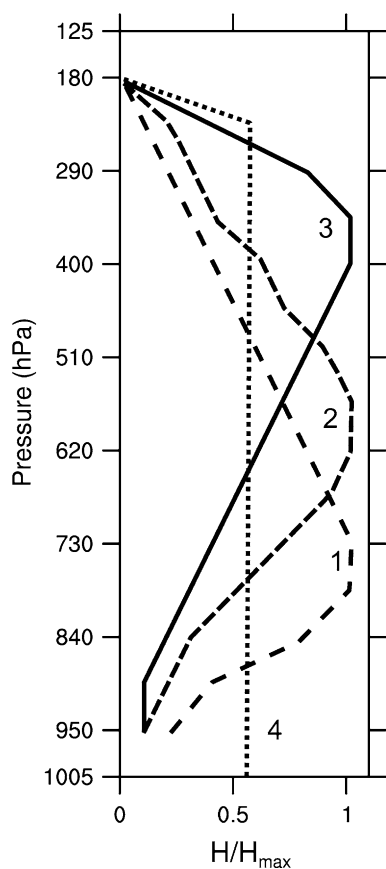


Fig. 14 Heating profiles (normalized by maximum) used in the solution to the eigenvalue problem described in the text (Sect. 5). (From 20)

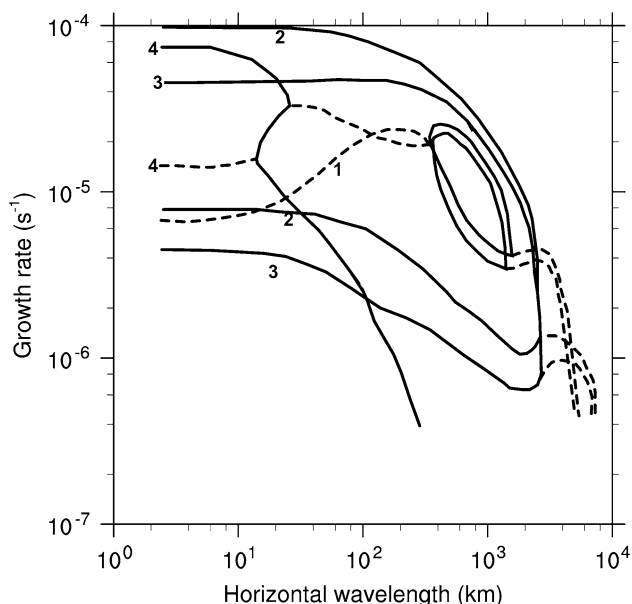


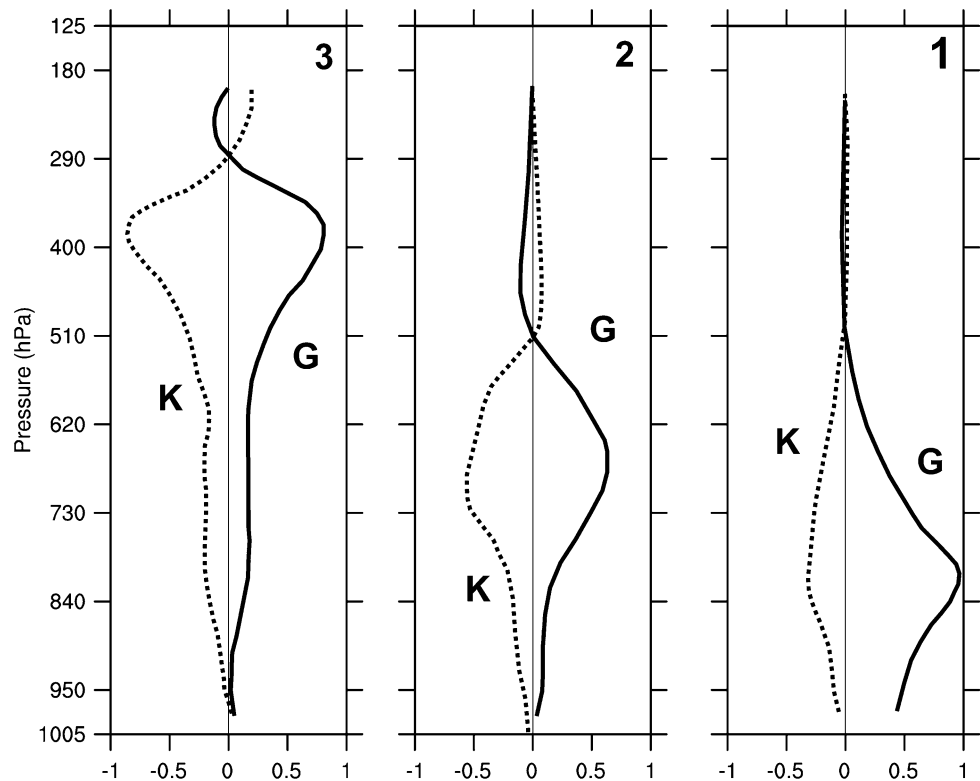
Fig. 15 Growth rates for unstable modes, with labels corresponding to those for the heating profiles in Fig. 11. Dashed curves represent oscillatory modes. (From 20)

mid-tropospheric heating generates a fast eastward propagating CISK mode, lower-tropospheric heating generates a stationary instead of a slow eastward propagating mode. They interpreted the slow MJO phase speed as a result of the interaction between the two modes. It is unclear whether these wave-CISK dynamics may explain what observed in our GCM simulations. In our model, when heating profiles are top heavy, there is no fast eastward propagating perturbation as in the three studies using wave-CISK models, and when the heating profile is bottom heavy, there is no stationary perturbations as in Chang and Lim (1988).

In a recent study of GCM simulations, Zhang and Mu (2005) found that an improvement of MJO simulation due to modifications in a cumulus parameterization is apparently related to changes in the behavior of simulated convective heating profiles. In their improved MJO simulation, there is clearly more abundant low-level (shallow) heating during the MJO transition periods that lead to convectively active phases. Their interpretation is that the modified cumulus parameterization makes deep convection more difficult to occur, leaving more chances for shallow convection, which is parameterized by a separated scheme. The improvement of the simulated MJO might have come from the promoted low-level heating. A major difference between their and our simulations is that the overall amount of shallow heating in their simulations remains roughly the same, no matter what cumulus parameterization was used. Shallow heating is only better “organized” into the MJO scale in their improved simulation. Regardless of whether the heating profiles were changed by careful tuning of cumulus parameterizations as in Zhang and Mu (2005) or were brutally forced upon the calculated convective heating term in the model as in this current study, results from both point to the potential role of bottom-heavy (low-level) heating in the dynamics of the MJO and in interpreting the difficulty many GCMs are facing in simulating a realistic MJO.

The importance of bottom-heavy heating to the MJO may come through its effect on low-level moisture convergence. The atmospheric large-scale divergent circulation in the tropics is sensitive to the vertical structure (or more specifically, the vertical gradient) of diabatic heating (e.g., Hartmann et al. 1984). It has been shown that the lower branch of the atmospheric circulation directly responding to the top-heavy heating profile is significant only in the lower troposphere away from the surface (Schneider and Lindzen 1977; Wu et al. 2000, 2001). Only if the heating profile peaks in the lower troposphere, can the atmospheric circulation respond with significant amplitude near the surface (Bergman and Hendon 2000; Schumacker et al. 2004). Such a low-level heating maximum is needed for the MJO if the feedback from its surface winds (through either its moisture convergence or evaporation) is crucial (Wu 2003).

Fig. 16 Generation of perturbation available potential energy (G) and conversion from perturbation available potential energy to perturbation kinetic energy (K) for unstable modes corresponding to the heating profiles in Fig. 11. The unit for the energy variable is $\text{m}^2 \text{s}^{-3}$. (From 20)



Low-level large-scale responses in the circulation to diabatic heating profiles indeed appear to be a reason for the difference between TH and BH. When bottom-heavy heating dominates in CT and BH, low-level moisture convergence is strong, deep coherent relative to heating regions, and exhibits large zonal scales (Fig. 17a, c). In contrast, when top-heavy heating dominates in TH, low-level moisture convergence becomes weak, shallow, and fragmental in its zonal scale (Fig. 17b). There is a perceptible sign of weak and shallow low-level moisture convergence immediately east of the main heating centers in CT and BH. This, consistent with one MJO theory in terms of boundary-layer frictional convergence (Wang 1988; Wang and Rui 1990), might be the reason for the eastward propagation promoted by bottom-heavy heating profiles.

If bottom-heavy heating profiles are crucial to MJO simulations, an inevitable question would be whether they exist in the real world. It is known that tropical convective heating is dominated by top-heavy profiles due to stratiform precipitation (Houze 1989). The early studies on the role of heating profile in the MJO struggled to justify the low-level heating maximum because of a lack of observed evidence for it. In fact, bottom-heavy heating profiles indeed exist in the tropics. Over the western Pacific, for example, apparent heating profiles (Q1, Yanai et al. 1973) derived from sounding observations are dominated by the top-heavy structure as manifested by the leading EOF

mode (Fig. 18). But, the second leading EOF mode is bottom heavy. Even though this second, bottom-heavy EOF mode only explains 10% of the total variance of the Q1 time series, in comparison to 74% variance explained by the first, top-heavy mode, this EOF analysis clearly shows that bottom-heavy heating profiles indeed exist and their importance might not be negligible. It is ensuring that such second, bottom-heavy EOF mode can be derived also from sounding observations taken in other tropical regions. A full report on this will be given separately. In short, the existence of bottom-heavy diabatic heating in the tropics is beyond doubt.

6 Summary

The most intriguing result from this study is that slow eastward propagation of intraseasonal perturbations resembling the MJO in a GCM can be produced only when there is sufficient bottom heavy (maximum in the lower troposphere) diabatic heating; when diabatic heating is top heavy (maximum in the upper troposphere) only, a stationary component dominated intraseasonal perturbations over the Indian and western Pacific Oceans. This result provides new modeling evidence for the importance of lower-tropospheric heating to the MJO, supporting similar results from previous studies (Li 1983; Lau and Peng 1987; Chang and Lim 1988; Sui and Lau 1989). But there are

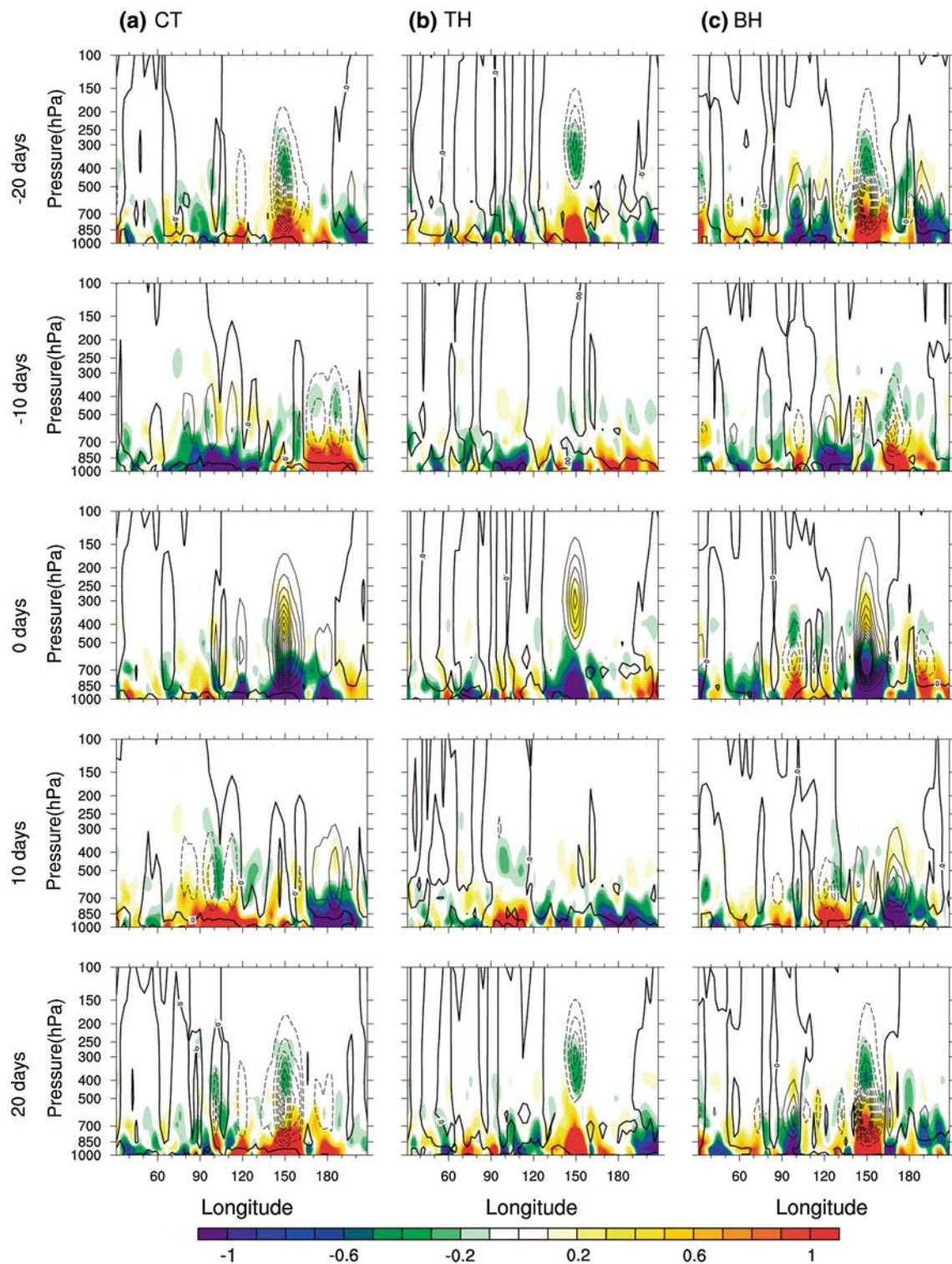


Fig. 17 Lag regression of intraseasonal (30–60 days) diabatic heating (contours, interval of 0.2 K/day) and moisture convergence (color, $10^{-6} \text{ g kg}^{-1} \text{ s}^{-1}$) upon maximum heating at 150°E (0 day) from CT (left column), TH (middle) and BH (right)

important distinctions between this and the previous studies using wave-CISK framework. First, there is no wave-CISK assumption made in our study. Second, the stationary intraseasonal perturbations are produced by top-heavy

heating profile only in our model, not in any of the wave-CISK models. It would be desirable, therefore, to reproduce and interpret our results using simple dynamical framework without any wave-CISK assumption. Third, the

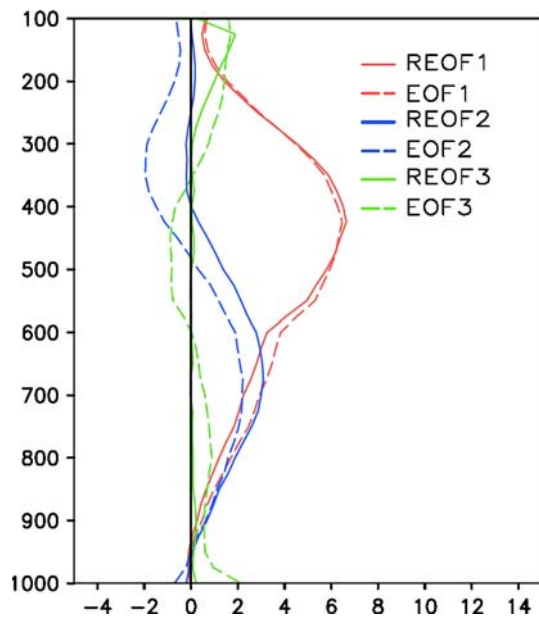


Fig. 18 First three leading modes of EOF (*dashed lines*) and rotated EOF (*solid lines*) analyses for apparent heating (Q1) profiles of TOGA-COARE (30)

previous studies mainly emphasized the dependence of the phase speed on the vertical scale in their interpretation of the sensitivity to the heating profile; an alternative interpretation has been presented in this study in terms of surface and low-level moisture convergence that is enhanced by bottom-heavy heating but weakened by top-heavy heating. Forth, we provide observational evidence for the bottom-heavy heating profile that is missing in the previous studies.

Possible reasons for bottom-heavy diabatic heating to play a critical role in our simulations to produce the MJO appear to come from its efficiency in promoting low-level moisture convergence, which in turn feeds back to deep convection. Such feedback has been suggested crucial to the MJO in theories (e.g., Wang 1988; Wang and Rui 1990). In consequence, a large-scale, deep, first-mode baroclinic circulation emerges, which is one of the fundamental signatures of the MJO. Low-level moisture convergence might have also been instrumental to the slow eastward propagation of the MJO. When heating profiles are top heavy, low-level moisture convergence is much weaker, moist convection also weaker and less organized on the large scale, the low- and upper-level circulations decoupled, and the signature of the MJO in the first-mode baroclinic structure lost. Some of these details might have been consequences of the particular way by which latent heating profiles were artificially modified or have been related to the particular cumulus parameterization used. Numerical experiments with less stringent test of the role of diabatic heating profiles in the MJO are needed to

confirm the results from this study. The biggest remaining uncertainty is why bottom-heavy heating profile would promote eastward propagation in our simulation. This uncertainty is inherently related to the lack of understanding of why the MJO propagates eastward at all. Based on the only observationally validated theory that provides an explanation for this zonal asymmetry in the MJO, namely, the frictional convergence theory (Wang 1988; Wang and Rui 1990), the promotion of the eastward propagation of the MJO in our simulation is through a stronger boundary-layer easterly wind response when diabatic heating is bottom heavy.

Based on the results from this study and discussion in Sect. 5, we propose the following hypothesis: The failure of global models to produce a realistic MJO is partially rooted in their insufficient diabatic heating in the lower troposphere. This hypothesis by no means dismisses the importance of deep convective heating, including its observed top-heavy structure, to the MJO (Lin et al. 2004). For example, the observed vertical structure of the MJO (e.g., Sperber 2003) is likely to be closely related to deep convective heating. A typical top-heavy heating profile would generate strong convergence in the mid troposphere (Bergman and Hendon 2000; Wu 2003), which tends to bring relatively dry air into convective region of the MJO. Dry air into convection regions is known to be detrimental to deep convection (e.g., Tompkins 2001). Taking convectively inactive and active phases as equally important components of the MJO, one can argue that top-heavy heating during active phases of the MJO might be necessary to the transition from active to inactive phases. The evolution from bottom-heavy to top-heavy heating profiles through the life cycle of the MJO in observations (e.g., Lin et al. 2006) and model simulations (Zhang and Mu 2005) might be an essential ingredient in the MJO dynamics. Such an evolution in the heating profile must have been distorted by the brute-force method used in our simulations. Nonetheless, the sensitivity demonstrated by the simulations with modified heating profile has exposed bluntly the possible role of bottom-heavy heating in the MJO. To completely understand the sensitivity of the simulated MJO to the vertical structure of convective heating, we need to consider more carefully designed numerical experiments and more advanced observations.

Acknowledgments The authors thank Brian Mapes, Eric Maloney, Paul Roundy, Jun-Ichi Yano and two anonymous reviewers for their comments on an earlier version of the manuscript. This study was support by the National Nature Science Foundation of China under grant no. 40575027 (Li, Jia, and Ling), by a grant from City University of Hong Kong under grant no. 7002329 (Zhou), and by US National Science Foundation under grant ATM0739402 (Zhang). Chidong Zhang thanks the Laboratory for Numerical Modeling for Atmospheric Sciences and Geophysical Fluid Dynamics (LASG), Institute of Atmospheric Physics, Chinese Academy of Sciences for

hosting his visits in 2006 and 2007, during which he collaborated with LASG scientists on this study.

References

- Bergman JW, Hendon HH (2000) Cloud radiative forcing of the low latitude tropospheric circulation: linear calculations. *J Atmos Sci* 57:2225–2245
- Bessafi M, Wheeler MC (2006) Modulation of south Indian Ocean tropical cyclones by the Madden–Julian Oscillation and convectively coupled equatorial waves. *Mon Weather Rev* 134:638–656. doi:10.1175/MWR3087.1
- Bond NA, Vecchi GA (2003) The influence of the Madden–Julian oscillation on precipitation in Oregon and Washington. *Weather Forecast* 18:600–613. doi:10.1175/1520-0434(2003)018<0600:TIOTMO>2.0.CO;2
- Chang C-P, Lim H (1988) Kelvin wave-CISK: a possible mechanism for the 30–50 day oscillation. *J Atmos Sci* 45:1709–1720
- Collins WD et al (2006) The community climate system model, version 3 (CCSM3). *J Clim* 19:2122–2143
- Crum FX, Dunkerton TJ (1992) Analytic and numerical models of wave-CISK with conditional heating. *J Atmos Sci* 49:1693–1708
- Edwards JM, Slingo A (1996) Studies with a flexible new radiation code. I: choosing a configuration for a large-scale model. *Q J R Meteorol Soc* 122:689–719. doi:10.1002/qj.49712253107
- Flatau M, Flatau PJ, Phoebus P, Niiler PP (1997) The feedback between equatorial convection and local radiative and evaporative processes: the implications for intraseasonal oscillations. *J Atmos Sci* 54:2373–2386. doi:10.1175/1520-0469(1997)054<2373:TFBECA>2.0.CO;2
- Frank WM, Roundy PE (2006) The role of tropical waves in tropical cyclogenesis. *Mon Weather Rev* 134:2397–2417. doi:10.1175/MWR3204.1
- Grabowski WW, Moncrieff MW (2005) Moisture-convection feedback in the tropics. *Q J R Meteorol Soc* 130:3081–3104. doi:10.1256/qj.03.135
- Hartmann DL, Hendon HH, Houze RA Jr (1984) Some implications of the mesoscale circulations in tropical cloud clusters for large-scale dynamics and climate. *J Atmos Sci* 41:113–121
- Hendon HH, Liebmann B (1990) The intraseasonal (30–50 day) oscillation of the Australian summer monsoon. *J Atmos Sci* 47:2909–2923
- Hendon HH (2000) Impact of air–sea coupling on the Madden–Julian oscillation in a general circulation model. *J Atmos Sci* 57:3939–3952
- Higgins RW, Shi W (2001) Intercomparison of the principal modes of interannual and intraseasonal variability of the North American monsoon system. *J Clim* 14:403–417. doi:10.1175/1520-0442(2001)014<0403:IOTPMO>2.0.CO;2
- Holtlag AAM, Boville B (1993) Local versus nonlocal boundary-layer diffusion in a global climate model. *J Clim* 6:1825–1842. doi:10.1175/1520-0442(1993)006<1825:LVNBLD>2.0.CO;2
- Houze RA Jr (1989) Observed structure of mesoscale convective systems and implications for large-scale heating. *Q J R Meteorol Soc* 115:425–461. doi:10.1002/qj.49711548702
- Hu Q, Randall DA (1994) Low-frequency oscillations in radiative-convective systems. *J Atmos Sci* 51:1089–1099. doi:10.1175/1520-0469(1994)051<1089:LFOIRC>2.0.CO;2
- Jia Xiaolong, *Numerical Simulations of the Tropical Intraseasonal Oscillation*, Doctor's thesis, Institute of Atmospheric Physics, Chinese Academy of Sciences, 2006
- Johnson RH, Rickenbach TM, Rutledge SA, Ciesielski PE, Schubert WH (1999) Trimodal characteristics of tropical convection. *J Clim* 12:2397–2418. doi:10.1175/1520-0442(1999)012<2397:TCOTC>2.0.CO;2
- Kalnay E, Kanamitsu M, Kistler R, Collins W, Deaven D, Gaudin L, Iredell M, Saha S, White G, Woollen J, Zhu Y, Chelliah M, Ebisuzaki W, Higgins W, Janowiak J, Mo K, Ropelewski C, Wang J, Leetnaa A, Reynolds R, Jenne R, Joseph D (1996) NCEP/NCAR 40-year reanalysis project. *Bull Am Meteor Soc* 77:437–471
- Kessler WS, McPhaden MJ, Weickmann KM (1995) Forcing of intraseasonal Kelvin waves in the equatorial Pacific. *J Geophys Res* 100:10613–10631. doi:10.1029/95JC00382
- Kiladis GN, Straub KH, Haertel PT (2005) Zonal and vertical structure of the Madden-Julian oscillation. *J Atmos Sci* 62:2809–2890. doi:10.1175/JAS3520.1
- Krishnamurti TN, Subrahmann D (1982) The 30–50 day mode at 850mb during MONEX. *J Atmos Sci* 39:2088–2095. doi:10.1175/1520-0469(1982)039<2088:TDMAMD>2.0.CO;2
- Lau KM, Chan PH (1986) Aspects of the 40–50 day oscillation during the northern summer as inferred from outgoing longwave radiation. *Mon Weather Rev* 114:1354–1367. doi:10.1175/1520-0493(1986)114<1354:AOTDOD>2.0.CO;2
- Lau KM, Peng L (1987) Origin of low-frequency (intraseasonal) oscillation in the tropical atmosphere, Part I: basic theory. *J Atmos Sci* 45:1781–1791. doi:10.1175/1520-0469(1988)045<1781:OTDOIO>2.0.CO;2
- Lau K-M, Shen S (1988) On the dynamics of intraseasonal oscillations and ENSO. *J Atmos Sci* 45:1781–1797. doi:10.1175/1520-0469(1988)045<1781:OTDOIO>2.0.CO;2
- Lawrence DM, Webster PJ (2002) The boreal summer intraseasonal oscillation: relationship between northward and eastward movement of convection. *J Atmos Sci* 59:1593–1606. doi:10.1175/1520-0469(2002)059<1593:TBSIOR>2.0.CO;2
- Li C (1983) Convection condensation heating and unstable modes in the atmosphere. *Chin J Atmos Sci* 7:260–268 in Chinese
- Li C (1985) Actions of summer monsoon troughs (ridges) and tropical cyclone over South Asia and the moving CISK mode. *Scientia Sin B* 28:1197–1206
- Li C, Zhou Y (1994) Relationship between intraseasonal oscillation in the tropical atmosphere and ENSO. *Chin J Geophys* 37:213–223 in Chinese
- Li C, Smith I (1995) Numerical simulation of the tropical intraseasonal oscillation and the effect of warm SSTs. *Acta Meteor Sin* 9:1–12
- Li C, Li G (1997) Evolution of intraseasonal oscillation over the tropical western Pacific/South China Sea and its effect to the summer precipitation in Southern China. *Adv Atmos Sci* 14:246–254. doi:10.1007/s00376-997-0053-6
- Li C, Long Z, Zhang Q (2001) Strong/weak summer monsoon activity over the South China Sea and atmospheric intraseasonal oscillation. *Adv Atmos Sci* 18:1146–1160. doi:10.1007/s00376-001-0029-x
- Li C, Long Z (2002) Intraseasonal oscillation anomalies in the tropical atmosphere and El Niño events. *Exchanges* 7(2):12–15
- Liebmann B, Hendon HH, Glick JD (1994) The relationship between tropical cyclones of the western Pacific and Indian Oceans and the Madden-Julian oscillation. *J Meteorol Soc Jpn* 72:401–411
- Lin J, Mapes BE, Zhang M, Newman M (2004) Stratiform precipitation, vertical heating profiles, and the Madden-Julian Oscillation. *J Atmos Sci* 61:296–309. doi:10.1175/1520-0469(2004)061<0296:SPVHPA>2.0.CO;2
- Lin J-L, Kiladis GN, Mapes BE, Weickmann KM, Sperber KR, Lin W et al (2006) Tropical intraseasonal variability in 14 IPCC AR4 climate models Part I: convective signals. *J Clim* 19:2665–2690. doi:10.1175/JCLI3735.1

- Lin X, Johnson RH (1996) Heating, moistening and rainfall over the western Pacific warm pool during TOGA COARE. *J Atmos Sci* 53:3367–3383. doi:10.1175/1520-0469(1996)053<3367:HMAROT>2.0.CO;2
- Maloney ED, Hartmann DL (1998) Frictional moisture convergence in a composite life cycle of the Madden-Julian Oscillation. *J Clim* 11:2387–2403. doi:10.1175/1520-0442(1998)011<2387:FMCIAC>2.0.CO;2
- Maloney ED, Hartmann DL (2000) Modulation of eastern North Pacific hurricanes by the Madden-Julian oscillation. *J Clim* 13:1451–1460. doi:10.1175/1520-0442(2000)013<1451:MOENPH>2.0.CO;2
- Maloney ED, Hartmann DL (2001) The sensitive of intraseasonal variability in the NCAR CCM3 to changes in convection parameterization. *J Clim* 14:2015–2034. doi:10.1175/1520-0442(2001)014<2015:TISOVI>2.0.CO;2
- Manabe S, Smagorinsky J, Strickler RF (1965) Simulated climatology of general circulation model with a hydrologic cycle. *Mon Weather Rev* 93:769–798. doi:10.1175/1520-0493(1965)093<0769:SCOAGC>2.3.CO;2
- Matsuno T (1966) Quasi-geostrophic motions in the equatorial area. *J Meteorol Soc Jpn* 44:25–43
- Matthews AJ (2004) Intraseasonal variability over tropical Africa during northern summer. *J Clim* 17:2427–2440. doi:10.1175/1520-0442(2004)017<2427:IVOTAD>2.0.CO;2
- Mo KC (2000) The association between intraseasonal oscillations and tropical storms in the Atlantic basin. *Mon Weather Rev* 128:4097–4107. doi:10.1175/1520-0493(2000)129<4097:TABIOA>2.0.CO;2
- Mu M, Li C (2000) The onset of summer monsoon over the South China Sea in 1998 and action of atmospheric intraseasonal oscillation. *Clim Environ Reserch* 5:375–387 in Chinese
- Paegle JN, Byerle LA, Mo KC (2000) Intraseasonal modulation of South American summer precipitation. *Mon Weather Rev* 128:837–850. doi:10.1175/1520-0493(2000)128<0837:IMOSAS>2.0.CO;2
- Raymond DJ (2001) A new model of the Madden-Julian oscillation. *J Atmos Sci* 58:2807–2819. doi:10.1175/1520-0469(2001)058<2807:ANMOTM>2.0.CO;2
- Schneider EK, Lindzen RS (1977) Axially symmetric steady-state models of the basic state for instability and climate studies. Part I. Linearized calculations. *J Atmos Sci* 34:263–279
- Sellers PJ, Min Y, Sud YC, Dalcher A (1986) A simple biosphere model (SIB) for use within general circulation models. *J Atmos Sci* 43:505–531. doi:10.1175/1520-0469(1986)043<0505:ASBMFU>2.0.CO;2
- Simmonds I (1985) Analysis of the “spinning” of a global circulation model. *J Geophys Res* 90:5637–5660. doi:10.1029/JD090iD03p05637
- Simpson J, Kummerow C, Tao W-K, Adler R (1996) On the tropical rainfall measuring mission (TRMM). *Meteorol Atmos Phys* 60:19–36. doi:10.1007/BF01029783
- Schumacher C, Houze RA Jr, Kraucunas I (2004) The tropical dynamical response to latent heating estimates derived from the TRMM precipitation radar. *J Atmos Sci* 61:1341–1358. doi:10.1175/1520-0469(2004)061<1341:TTDRTL>2.0.CO;2
- Slingo A (1980) A cloud parameterization scheme derived from GATE data for use with a numerical model. *Q J R Meteorol Soc* 106:747–770. doi:10.1002/qj.49710645008
- Slingo A (1987) The development and verification of a cloud prediction scheme for the ECMWF model. *Q J R Meteorol Soc* 113:899–927. doi:10.1256/smsqj.47708
- Slingo, J. M. and Coauthors, Intraseasonal oscillations in 15 atmospheric general circulation models: Results from an AMIP diagnostic subproject. *Climate Dyn.*, 1996, 13: 325–357. doi:10.1007/BF00231106
- Slingo JM, Inness P, Neale R, Woolnough S, Yang G-Y (2003) Scale interactions on diurnal to seasonal timescales and their relevance to model systematic errors. *Ann Geophys* 46:139–155
- Sperber KR (2003) Propagation and the vertical structure of the Madden-Julian Oscillation. *Mon Weather Rev* 131:3018–3037. doi:10.1175/1520-0493(2003)131<3018:PATVSO>2.0.CO;2
- Sperber KR (2004) Madden-Julian variability in NCAR CAM 20 and CCSM2.0. *Clim Dyn* 23:259–278. doi:10.1007/s00382-004-0447-4
- Sperber KR, Gualdi S, Legutke S, Gayler V (2005) The Madden-Julian oscillation in ECHAM4 coupled and uncoupled GCMs. *Clim Dyn* 25:117–140
- Sui C-H, Lau K-M (1989) Origin of low-frequency (intraseasonal) oscillations in the tropical atmosphere. Part. II: Structure and propagation of mobile wave-CISK modes and their modification by lower boundary forcings. *J Atmos Sci* 46:37–56
- Tiedtke M (1989) A comprehensive mass flux scheme for cumulus parameterization in large-scale models. *Mon Wea Rev* 117:1779–1800
- Tompkins AM (2001) Organization of tropical convection in low vertical wind shears: the role of water vapor. *J Atmos Sci* 58:529–545. doi:10.1175/1520-0469(2001)058<0529:OOTCIL>2.0.CO;2
- Waliser DE, Lau KM, Kim JH (1999) The influence of coupled sea surface temperatures on the Madden-Julian oscillation: a model perturbation experiment. *J Atmos Sci* 56:333–358. doi:10.1175/1520-0469(1999)056<0333:TIOCSS>2.0.CO;2
- Waliser DE, Lau KM, Stern W, Jones C (2003) Potential predictability of the Madden-Julian Oscillation. *Bull Am Meteorol Soc* 84:33–50. doi:10.1175/BAMS-84-1-33
- Wang B (1988) Dynamics of tropical low-frequency waves: an analysis of the moist Kelvin wave. *J Atmos Sci* 45:2051–2065. doi:10.1175/1520-0469(1988)045<2051:DOTLFW>2.0.CO;2
- Wang B (2005) Theory, 307–360. In: Lau WKM, Waliser DE (eds) Intraseasonal variability of the atmosphere–ocean climate system. Praxis, Chichester, pp 436
- Wang B, Rui H (1990) Synoptic climatology of transient tropical intraseasonal convective anomalies: 1975–1985. *Meteorol Atmos Phys* 44:43–61. doi:10.1007/BF01026810
- Wang W, Schlesinger ME (1999) The dependence on convective parameterization of the tropical intraseasonal oscillation simulated by the UIUC 11-layer atmospheric GCM. *J Clim* 12:1423–1457. doi:10.1175/1520-0442(1999)012<1423:TDOCPO>2.0.CO;2
- Wang Z-Z, Wu G-X, Liu P, Wu T-W (2005) The development of Goals/LASG AGCM and its global climatological features in climate simulation I-influence of horizontal resolution. *J Trop Meteorol* 21(3):225–237 In Chinese
- Wheeler M, Kiladis GN (1999) Convectively coupled equatorial waves: analysis of clouds and temperature in the wavenumber-frequency domain. *J Atmos Sci* 56:374–399
- Wheeler MC, Hendon HH (2004) An all-season real-time multivariate MJO index: development of an index for monitoring and prediction. *Mon Weather Rev* 132:1917–1932. doi:10.1175/1520-0493(2004)132<1917:AARMMI>2.0.CO;2
- Wheeler MC, McBride JL (2005) Intraseasonal variability in the atmosphere–ocean climate system. In: Lau WKM, Waliser DE (eds) Praxis, Chichester, pp 125–173
- Wu G-X, Liu H, Zhao Y-C and Li W-p, (1996) A nine-layer atmospheric general circulation model and its performance. *Adv Atmos Sci* 13(1):1–18. doi:10.1007/BF02657024
- Wu G, Zhang X, Liu H, Yu Y, Jin X, Guo Y, Sun S, Li W, Wang B, Shi G, 1997 Global ocean-atmosphere-land system model of LASG (GOALS/LASG) and its performance in simulation study, *Quart. J. Appl. Meteor.*, Supplement Issue, 15–28. (In Chinese)

- Wu Z (2003) A shallow CISK, deep equilibrium mechanism for the interaction between large-scale convection and large-scale circulations in the tropics. *J Atmos Sci* 60:377–392. doi:10.1175/1520-0469(2003)060<0377:ASCDEM>2.0.CO;2
- Wu Z, Sarachik ES, Battisti DS (2000) Vertical structure of convective heating and the three-dimensional structure of the forced circulation on an equatorial beta plane. *J Atmos Sci* 57:2169–2187. doi:10.1175/1520-0469(2000)057<2169:VSOCHA>2.0.CO;2
- Wu Z, Sarachik ES, Battisti DS (2001) Thermally driven tropical circulations under Rayleigh friction and Newtonian cooling: analytic solutions. *J Atmos Sci* 58:724–741. doi:10.1175/1520-0469(2001)058<0724:TDTCUR>2.0.CO;2
- Xie P, Arkin PA (1997) Global precipitation: a 17-year monthly analysis based on gauge observations, satellite estimates, and numerical model outputs. *Bull Am Meteor Soc* 78:2539–2558
- Xue Y, Sellers PJ, Linter JL, Shukla J (1991) A simplified biosphere model for global climate studies. *J Clim* 4:345–364. doi:10.1175/1520-0442(1991)004<0345:ASBMFG>2.0.CO;2
- Hui Yang, Chongyin Li (2003) The relation between atmospheric intraseasonal oscillation and summer severe flood and drought in the Changjiang-Huaihe basin. *Adv Atmos Sci* 20:540–553. doi:10.1007/BF02915497
- Yanai M, Esbensen S, Chu J-H (1973) Determination of bulk properties of tropical cloud clusters from large-scale heat and moisture budgets. *J Atmos Sci* 30:611–627
- Zhang C (2005) 2005: Madden-Julian Oscillation. *Rev Geophys* 43:RG2003. doi:10.1029/2004RG000158
- Zhang GJ, McFarlane NA (1995) Sensitivity of climate simulations to the parameterization of cumulus convection in the CCC-GCM. *Atmos Ocean* 3:407–446
- Zhang C, Gottschalck J (2002) SST anomalies of ENSO and the Madden-Julian Oscillation in the equatorial Pacific. *J Clim* 15:2429–2445. doi:10.1175/1520-0442(2002)015<2429:SAOEAT>2.0.CO;2
- Zhang C, Dong M, Gualdi S, Hendon HH, Maloney ED, Marshall A, et al (2006) Simulations of the Madden-Julian oscillation in four pairs of coupled and uncoupled global models. *Clim Dyn* 27:573–592. doi:10.1007/s00382-006-0148-2
- Zhang G, Mu M (2005) Simulation of the Madden-Julian oscillation in the NCAR CCM3 using a revised Zhang–McFarlane convection parameterization scheme. *J Clim* 18:4046–4064. doi:10.1175/JCLI3508.1